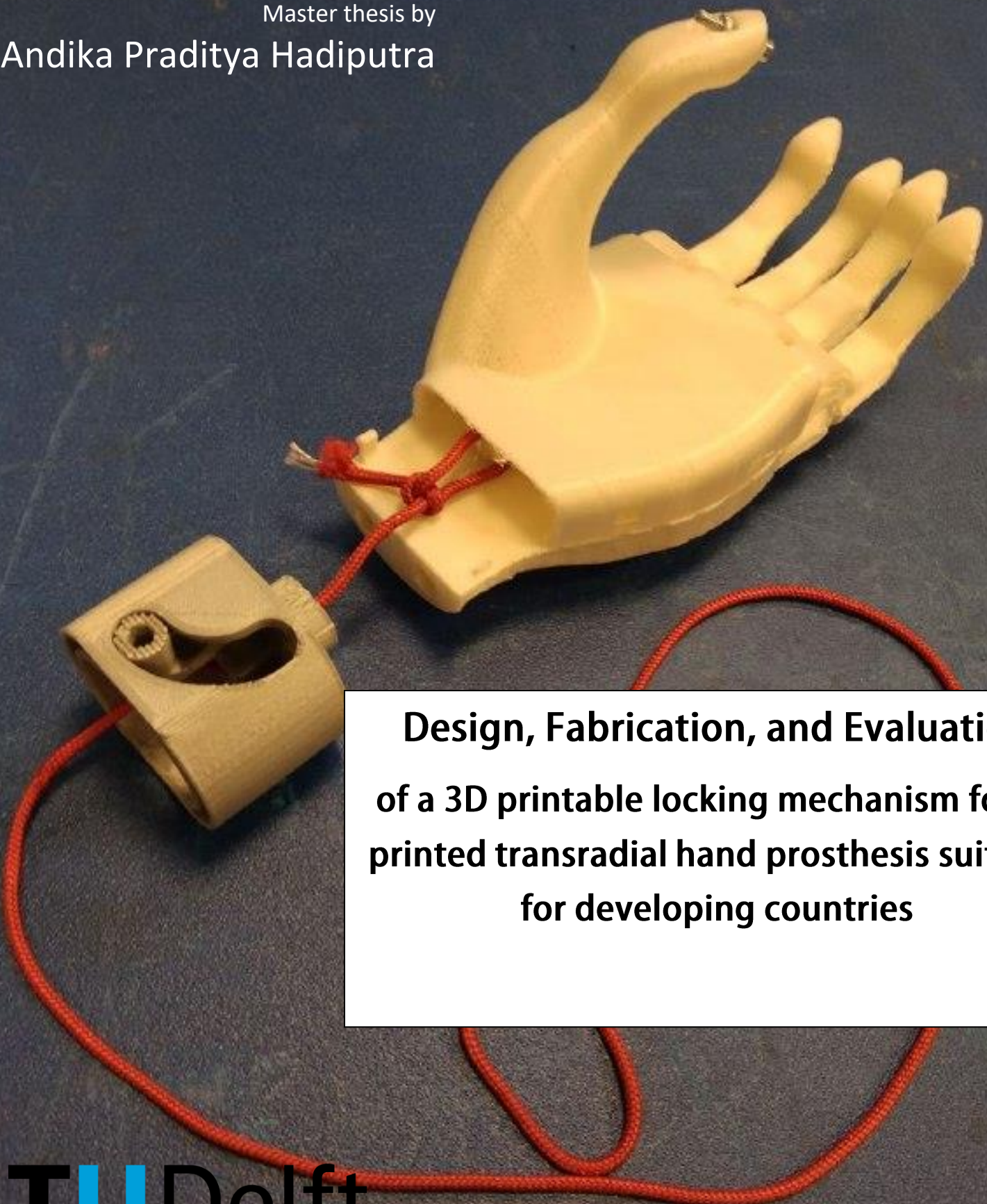


Master thesis by
Andika Praditya Hadiputra

A 3D printed yellow hand prosthesis is shown against a dark blue background. The prosthesis is a transradial hand, featuring a wrist, palm, and five fingers. A red rope is attached to the wrist area, extending to a separate 3D printed component. This component is a locking mechanism, which is a rectangular block with a circular opening and a gear-like structure inside. The rope is threaded through this mechanism. The entire assembly is designed for use in developing countries.

**Design, Fabrication, and Evaluation
of a 3D printable locking mechanism for 3D
printed transradial hand prosthesis suitable
for developing countries**

Design, fabrication, and evaluation, of a 3D printable locking mechanism for 3D printed transradial hand prosthesis suitable for developing countries

Andika Praditya Hadiputra

To obtain the degree of Master of Science

At the Delft University of Technology,

To be defended publicly on Monday November 19th 2018 at 09.30 AM

Student number: 4625145

Project duration: April 2018 – November 2018

Thesis Committee:

Dr. ir. Dick H. Plettenburg

3me TU Delft, chair

Dr. ir. Gerwin Smit

3me TU Delft, supervisor

Juan S. Cuellar Lopez, MSc

3me TU Delft, supervisor



Abstract

Voluntarily closing body-powered (BP) prosthesis is generally accepted as a low-cost solution for upper limb amputation and is more suitable for the amputation problem in the developing countries. Utilization of a locking mechanism is beneficial to lessen patient's fatigue which is usually presents in the operation of a voluntarily closing body-powered prosthesis.

Unfortunately, commercial prosthesis locking mechanism are still susceptible to force-drop in its pinching up to 90% of original force. Moreover, exporting commercial prosthesis locking mechanism into a wide range of area in developing countries can be a challenge due to various factors (e.g., the low accessibility of an appropriate medical center, lack of specialized personnel, and general logistical problems of the devices).

To solve this problem, we propose to utilize a 3D printed the locking mechanism of a hand prosthesis. Thus, the goal of this project is to design, fabricate, and evaluate a 3D printable locking mechanism for 3D printed transradial BP prostheses for developing countries.

We examine the state of the art of 3D printing to select appropriate process and material and the patents regarding locking mechanism and prosthesis to select the appropriate proof of concepts for locking mechanism. We select the best proof of concepts using Harris's profile with the design criteria adopted from prosthesis's user basic requirement extracted from the scientific literature. In the end, we choose self-energizing brake concept for the locking mechanism, PLA for the material, and FDM for the 3D printing process.

We fabricated the locking mechanism in 1 assembly direct after printing using a non-assembly mechanism. After using spring as the mean of evaluation, this mechanism can hold up to around 75 N force from the hand using polypropylene wire. Using TRS Hook, the locking mechanism experienced less than 1 N force drop if we use the hook to give 15 N pinching force and around 12 N force drop if we give 45 N pinching force. This value varies with the wire material utilized

Preface

Its been more than 2 years since I live here in the beautiful Netherlands, surely there are many amazing things I experienced here both as an engineer and as a person. I am very grateful to The One and Only God almighty for the opportunity to learn here at Delft University of Technology. I would also like to thank my family, especially my parents for always supporting me and keep communicating often, and also helps me whenever I have personal trouble.

All of my effort here is always with the motif to learn as much as I can for then used this knowledge to contribute back home in Indonesia afterwards. This driving force keeps me straight in time when I am faced with numerous doubts along the way. Also, for all of my colleague from Indonesia who endure this hardship together, there will be difficult time back home, but I believe we can thrive together and bring this nation to glory as long as we believe.

I first came to know this project from my colleague, which then introduced me to my daily supervisor Juan. I see his noble cause really inspiring and motivating to me, as a person with similar motivation to work for his country. Juan has been really a great partner to consult regarding the project. As I often just walks in to his office and just casually took his time, I will say million thanks and sorry for the inconveniences. I will be really looking forward for the outcome of the project as I believe there is more I can learn afterwards

Afterwards, Juan involve Gerwin to the project as he become my supervisor. I have also million of gratitude that words cannot explain to Gerwin. Thank you for all the critical thought you gave me along the project. You thought me on how to be critical, tidy, and systematic on doing work. Lastly, I never have the opportunity to say congratulation on the twins. I hope for the best for both you and your family.

And for Dick, while being the last person I came to, I would still thank you for the insight you give to this project. Personally, I will be thanking you more because you take care of us BME Student on our first year. Also your lecture on biomedical design greatly helps my thought process in this project.

Contents

Abstract	2
Preface.....	3
Contents	4
List of Figures.....	6
List of Tables	8
1. Introduction.....	9
1.1 Background problem	9
1.2 Problem definition.....	11
1.3 Goal.....	11
2. Outline	12
3. State of the art.....	14
3.1 3D printers' specifications	14
3.2 Mechanical properties of common 3D Printing material	16
3.2.1 Material from photopolymer 3D printers	16
3.2.2. Material from powder-based 3D printers	16
3.2.3 Material from molten-based 3D printers	18
3.4 Non-assembly mechanism.....	20
3.3 Body-powered prosthesis basic user requirements.....	22
3.3.1 Control.....	22
3.3.2 Cosmesis	22
2.3.3 Comfort.....	22
3.3.4 Durability	23
3.5 Discussion	23
3.5.1 Process and material selection.....	26
3.5.2 Design constraint and design criteria	27
4. Design of the locking mechanism.....	29
4.1 Cable-Related Locking Mechanism from patent search.....	23
4.2 Conceptual solution and winning concept.....	29
4.3 Initial screening	30
4.4 Shape lock directly through the cable	30
4.5 Shape lock using a cable that is mounted in a winch	36

4.5.1 With Gear Bearing	39
4.5.2 Without gear bearing	42
4.6 Discussion	43
4.6.1 Selection Winning Concept	44
4.6.2 Assessing the Critical Components from the self-energizing solution	44
5. Optimization of the Locking mechanism	46
5.1 Methodology	46
5.2 Result	47
5.2.1 The effect of the build direction.....	47
5.2.3 The effect of surface topology on the performance.	49
5.2.4 The effect of different cable material	51
5.3 Discussion	54
6. Prototype design	55
6.1 Frame.....	55
6.2 Handle.....	56
6.3 Parametric input.....	57
6.4 3D printing process.....	60
7. Evaluation of the final prototype and Discussion.....	61
7.1 Methodology	61
7.2 Result	62
7.2.1 15N pinch force	62
7.2.2 45N pinch force	64
7.3 Discussion	65
8. Conclusion	66
8.1 Future works.....	66
Appendix.....	67
References.....	67
3D printing process parameter.....	70
Python code for the design	71
Part Drawings (next page)	Error! Bookmark not defined.

List of Figures.

Figure 1. Voluntarily Closing Body Powered Prosthesis].....	10
Figure 2. Overall Project's Flowchart.....	13
Figure 3. Microstructure of a SLS 3D-printed product [28].....	17
Figure 4. Anisotropy due to the raster angle of the specimens [32].....	18
Figure 5. Air gap from a test specimen [30].....	19
Figure 6. A range of examples of rigid joints with various DoF [44].....	20
Figure 7. Support generation on a shaft-inside-a-hole hinders the mobility of the shaft itself [43].	21
Figure 8. Examples of compliance joints [47].....	21
Figure 9. Print direction and the loading condition for identifying the fatigue limit of PLA [51]	26
Figure 10. Example of cable locked through an interface. Here the cable (17) is locked in its place via a pawl (28) and a ratchet (22) [43].	24
Figure 11 left: Locking the cable (120) directly with a cam 608 [44] ; right: Locking the cable (72) via a winch (59) [45].....	24
Figure 12. Self-energizing brake concept drawing. Here the force that happen due to the hand wanting to open is transmitted through the cable and “energizes” the locking bar by pressing the locking bar to the cable itself creating normal force that is necessary for the lock.	31
Figure 13. Beam equation for the locking ban. The force acting on the beam is the cosine of the hand force due to the locking bar start to lock at a certain angle, not all the way at 90 degree	32
Figure 14. Global CAD for the self-energizing and the realization of the concept.....	33
Figure 15. Stress analysis in the shaft area	35
Figure 16. Force analysis in a capstan device	36
Figure 17. Optimal design for the end part of the winch	37
Figure 18. Anatomy and term used in gears	37
Figure 19. Table of standard gear proportion [48]	38
Figure 20. Left: Global Cad for the gear bearing. Right: Emmet Lalish’s parametric design for the gear bearing..	39
Figure 21. Orientation view for the global CAD	40
Figure 22. Realization of the concept.....	40
Figure 23. Critical components for the winch	41
Figure 24. Exploded view of the solution without bearing	42
Figure 25. Critical components for the winch without the gear bearing	42
Figure 26. The shear force experienced in the shaft.....	43
Figure 27. Part-to-part relationship in the locking mechanism	45
Figure 28. Functional flow in the form of mechanical force	45
Figure 29. Schematic overview of the test bench	46
Figure 30. Actual picture of the test bench; (1) Load cell (for calibration), (2) Locking mechanism sample, (3) Redboard, (4) Load cell driver, (5) spring, (6) load cell	47
Figure 31. Part display for two different build orientation in the slicer software. Left is for vertical build, and right for horizontal build.....	48
Figure 32. Printing result for two different build direction. Specimens on the top picture were horizontally build and specimen on the bottom were vertically build	48
Figure 33. Force retained by the spring across different specimen with different surface topology.....	50
Figure 34. Geometry to increase surface friction, normalized for force retained percentage.....	51

Figure 35. DG performance with nylon and fishing wire.....	52
Figure 36. Visible deformation in the fishing wire	53
Figure 37. Maximum performance from DG specimen with respect to different wire material.....	53
Figure 38. DINED2004 Dutch adult database	55
Figure 39. Initial frame design.....	55
Figure 40. Handle design A.....	56
Figure 41. Handle design B.....	56
Figure 42. Full prosthesis system for right hand (orange = hand, teal = frame, green = handle, white = cable)....	57
Figure 43. Section view of the locking mechanism	57
Figure 44. Input design parameter and their corresponding output	58
Figure 45. Example of different parameter input (HT,HW, and offset)	58
Figure 46. Effect of nozzle size to the clearance (left = 0.1 mm nozzle size, right = 0.4 mm nozzle size).....	59
Figure 47. Height difference for the locking bar	59
Figure 48. Realization of the full prototype	59
Figure 49. Test bench used for the final evaluation.....	61
Figure 50. Activation force vs pinch force diagram of sample printed using polypropylene wire and nylon 2 wire. (1) set the activation force to acquire 15 N pinch force (2) engage the lock (3) release the activation force, (4) reapply the activation force and release locking the mechanism.....	62
Figure 51. Performance of this locking mechanism in comparison with several commercially available locking mechanism (source : [11], minus the error bar.).....	63
Figure 52. Result of 45N pinch force test. (a) for this 3D printed locking mechanism, (b) the result of Gemmell's experiment [10] . (1) Start giving activation force (2) finger close and start to give pinch force as we further increase the activation force (3) locking is engaged, removal of the activation force (4) reapply the activation force to release locking the mechanism (not applicable to the capstan lock). (5) Decreasing the activation force. (6) finger open.....	64

List of Tables

Table i. Per capita incidence of traumatic amputation in several countries [1]	9
Table ii. Comparison for each 3D printing processes [20].....	15
Table iii. Summary of the mechanical properties from common resins [21].....	16
Table iv. Mechanical properties of nylon-based SLS 3D printing materials [25].....	17
Table v. Mechanical properties of metal-based SLS 3D printing materials [26]	17
Table vi. Summary of the mechanical properties of every common molten-based materials [31].....	19
Table vii. Classifying our findings from the patent search	25
Table viii. Initial concept solution for the locking device	29
Table ix. Possible configurations using different value of r for the radius of the locking bar.....	34
Table x. Possible configurations using a different value of r for the shaft.....	36
Table xi. Gear specifications utilized with the reasons	38
Table xii. The maximum allowable force with the relation of the gear's width is	39
Table xiii. Design criteria of the 3 solutions.	44
Table xiv. Components of the test bench.....	47
Table xv. Measurement result for vertical build and horizontal build specimens pulled to 20N of spring force...	49
Table xvi. Specimen's codename and CAD picture.....	50
Table xvii. Wire specification	52
Table xviii. Minimum and Maximum value of several parameters for the parametric design	55
Table xix. Z-Support possible configuration in Cure (support is represented in blue lines)	60
Table xx. Specification for the 2nd test bench	62

1

1. Introduction

1.1 Background problem

Amputation occurs more in the developing countries in comparison to the developed countries. Staats argued that there are several major factors that cause an amputation that is more prevalent in developing countries^[1]:

- Landmines due to a time /post-war condition.
- Traffic incidence due to poor vehicle and safety
- Biological incidence (snakebites, infections, etc.) in conjunction with poor medical infrastructure that hardly compensates emergency situations.

Staats also provided an example of a comparison of amputation due to trauma between developed and developing countries in this matter, which can be seen in Table i. Other studies that were held locally reported a similar conclusion about amputation due to trauma in developing countries such as India, Nigeria, South Korea, and Iran^[2-5].

Table i. Per capita incidence of traumatic amputation in several countries [1]

Cambodia	1 per 256 people
Angola	1 per 470 people
Somalia	1 per 1000 people
Vietnam	1 per 2500 people
USA	1 per 22,000 people

In the literature review, Carey and her team found that voluntarily closing body-powered (BP) prosthesis is generally accepted as a low-cost solution for upper limb amputation compared to myoelectric prosthesis^[6]. This low-cost solution, thus, is considered as an ideal solution amputation problem in developing countries^[7,8]. However, prosthesis user reported that they often experienced fatigue on a daily basis when using their prosthesis^[9]. One solution to address this problem is to utilize a locking mechanism to lock the operating cable tension. Although utilizing a locking mechanism can reduce the functionality score of the subjects, it is proven to lessen the energy required from them to perform the test^[10].

However, a major problem still remains regarding locking mechanism as Smit and Plettenburg reported that a prosthesis fitted with locking mechanism still susceptible to a force-drop up to 90% of its initial force after activation^[11]. Nevertheless, even if we assume current locking mechanism devices are sufficient, exporting them into a wide range of area in developing countries can be a challenge due to various factors (e.g., the low

accessibility of an appropriate medical center [12], lack of specialized personnel[13], and general logistical problems of the devices [14]). Keep in mind that the logistical challenge can expand beyond the locking mechanism, as prosthesis usually come in several different parts (e.g., hand, wrist unit, terminal)

One solution to address both of the logistic problems and the force-drop problem is to manufacture the entire hand prosthesis system via 3d printing locally, including a new 3D printable locking mechanism. Several publications reported that incorporating 3D printing into various framework can result in several benefits for developing countries such as; increasing living standards and providing a higher quality of healthcare [15], and providing equipment to deprived schools and universities [16]. This project aims, thus, aims to design a locking mechanism that solves both the force drop and the logistical problem exist in a developing country by taking an advantage of a 3D printing processes



Figure 1. Voluntarily Closing Body Powered Prosthesis]

1.2 Problem definition

Based on the previous explanation, we propose our problem definition as follow:

- Using a voluntarily closing body powered prosthesis with locking mechanism still yeilds in a relatively large force drop on its pinching force
- Logistical challenge for distributing commercial locking mechanism to developing countries

1.3 Goal

This project's goal is to design, fabricate, and evaluate a 3D printable locking mechanism for 3D printed transradial BP prostheses that is suitable for developing countries. With this project, we are aiming to design and fabricate a 3D printable locking mechanism that is not suspected to a large amount of force drop and complies to limitations that might be presents in developing countries.

2

2. Outline

This report is divided into 8 chapters. We will explain the purpose of each chapter in this chapter:

In Chapter 3, we will examine the state of the art of 3D printing and patient's requirement for a hand prosthesis. After examination, we will present design criteria that correspond to the patient's requirement, and design constraint that corresponds with the available 3D printing technology. We will also examine various relevant patents.

In Chapter 4, we will start the design process of the locking mechanism. We will categorize the result of the patent search and try to come up with conceptual solutions that correspond them. Lastly, we will test each conceptual solution using the design criteria that we propose in Chapter 3.

In Chapter 5, we will try to optimize the locking mechanism, so they have a better performance.

In Chapter 6, we will design the prototype using the best design we came up from chapter 5.

Lastly, in Chapter 7, we will evaluate the prototype and compare them with the performance of various existing locking mechanism.

Figure 2 summarized the project in the form of a flowchart.

Project Flow

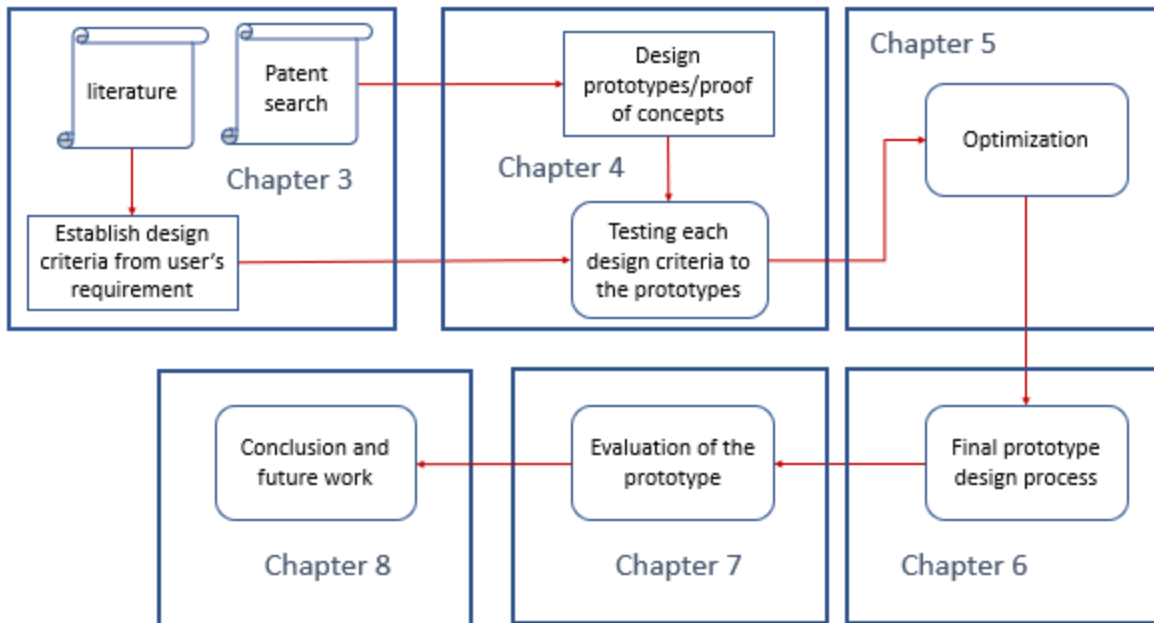


Figure 2. Overall Project's Flowchart

3

3. State of the art

3.1 3D printers' specifications

Additive manufacturing, or widely known as 3D printing, is a relatively new manufacturing technique performed by additively make the product in a layer-by-layer fashion. It's a fundamentally different technique compared to the traditional manufacturing processes (e.g., mill, lathe, etc.) which are subtractive in nature. In a simplified nature, the process of 3D printing a part starts from designing it in CAD, transferring the design to stereolithography format (.stl), and having the printer translate the .stl into a real part with a physical body.

In his book, Gibson et al. categorized 3D printing into 4 different variations^[17]:

1. Photopolymer-based system

In this system, the solid part is created from a hardened photopolymer resin. The resin is hardened at a certain position via a compatible light source. The print can be in a normal sequence or in a bottomed-up sequence, as can be seen in Figure 2. The resolution of the object depends on the wavelength of the light used to harden the resin (usually is UV). As a result, generally photopolymer-based 3D printing results in objects with excellent precision

2. Powder-based system

In this system, the solid part is created from solidifying material powder using a specific heat source. The heat source solidifies the material via either sintering or melting the powders. The precisions of the object depend on the precision of the heating system.

3. Molten material system

In this system, the solid part is created from a solidified molten material. Firstly, the printer heats up the material into its molten state. Afterward, the printer will deposit the material into a specific location, which then will solidify at the room temperature. As such, the part's precision depends on the precision of the printer itself to deposit the material. One common 3D printer utilizing this system is FDM printers (fused deposition modeling). FDM is the most common printer out of all 3D printing system.

4. Solid sheets system

In this system, the solid part is created from several solid sheets which are stacked and shaped accordingly. The stacking sheets are then bonded together using a heat-activated resin.

To determine the suitable 3D printing processes for this project, we will compare each variation in Table ii. The data we provide in this table was initially created by 3dhubs.com and has been reviewed by more than 10,000 verified owners (<https://www.3dhubs.com/best-3d-printer-guide>). From this info, we acquired the design constraint in term of resolution and volume.

Table ii. Comparison for each 3D printing processes [20]

process		Machines	support	resolution	Build Volume Approximation	price range
Photolymer based	SLA + DLP	9	support less	6 - 32 microns	6.4 × 13.4 × 4 cm to 150 × 55 × 75 cm	2.8k \$ - 200k \$
Powder based	SLS	6	powder as support	60-100 microns	10 × 13 × 10 cm to 70 × 58 × 38 cm	17k \$ - 250k \$
	Metal sintering	1	powder as support	n/a	14 × 10 × 14 cm	n/a
Molten Material Based	FDM	108	allowed	100-300 microns	10 × 10 × 10 cm to 100 × 120 × 100 cm	210 \$ - 15k \$
	CFF	3	allowed	50-100 microns	around 33 x 25 x 20 cm	3.5k \$ - 70k \$
	Jetting	3	allowed	16-100 microns	around 25.4 × 20.3 × 38.1 cm	60k \$ - 70k \$
	Polyjet	2	allowed	16-100 microns	25.5 × 20 × 25.2 cm and 30 × 15 × 20 cm	20k \$ - 25k \$
Sheet Based	n/a	n/a	n/a	n/a	n/a	n/a

3.2 Mechanical properties of common 3D Printing material

3.2.1 Material from photopolymer 3D printers

Due to the varying factor affecting mechanical properties from curing a photopolymers [17], it is challenging to have a precise mechanical properties consideration from just the material itself. To help us, 3dhubs.com had compiled a summary of the mechanical properties of several common resins. We prefer this reference over those from the academic literature due to: (a) the limitation of available academic literature regarding this issue and (b) the data is sourced from various commercially available resin. The literature showed that SLA 3D printing processes would result in a broadly isotropic product [18-20]. Table iii shows the summary of materials used in SLA 3D printing

Table iii. Summary of the mechanical properties from common resins [21]

	Resin type				
	Standard & Clear	Tough	Durable	Heat resistant	Ceramic reinforced
IZOD impact strength (J/m)	25	38	109	14	N/A
Elongation at break (%)	6.2	24	49	2	5.6
Tensile strength (MPa)	65	55.7	31.8	51.1	75.2
Tensile Modulus (GPa)	2.8	2.8	1.26	3.6	4.1
Flexural Modulus (GPa)	2.2	1.6	0.82	3.3	3.7
HDT @ 0.45 MPa (°C)	73	48	43	289	88

3.2.2. Material from powder-based 3D printers

Like photopolymer, the mechanical properties of powder-based 3D printing materials depend greatly on the local processes condition [21]. On the other hand, unlike photopolymers, powder-based 3D printing processes result in anisotropic products. As can be seen from Figure 3, there are non-homogeneity in the microstructure of an SLS printed parts, which leads to its anisotropic nature. For the sake of comparison, we will use the mechanical properties provided by the material supplier in Table iv and Table v. In the case of the mechanical properties of metal 3D printing materials, we use a property provided by a supplier due to insufficient information from the academic literature

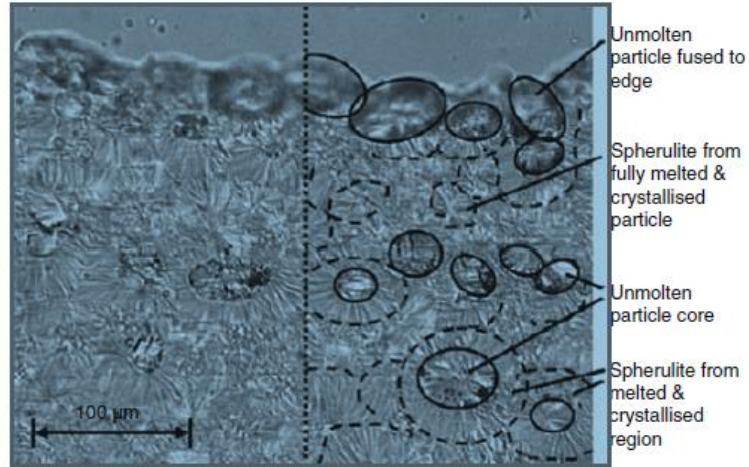


Figure 3. Microstructure of a SLS 3D-printed product [28]

Table iv. Mechanical properties of nylon-based SLS 3D printing materials [25]

	Nylon-based material				
	General purpose nylon PA 22100	Biocompatible nylon PA 2221	glass bead filled nylon PA 3200GF	Aluminum filled nylon	Polyaryletherketone, PEEK HP3
Density (g/cm ³)	0.93	0.93	1.22	1.36	1.32
Elongation at break (%)	6	24	10	9	4
Tensile strength (MPa)	48	44	51	48	90
Tensile Modulus (GPa)	1.7	1.6	3.2	3.8	4.2
HDT @ 0.45 MPa (°C)	163	157	166	169	165

Table v. Mechanical properties of metal-based SLS 3D printing materials [26]

	Metal-based material		
	Aluminum (AlSi10Mg)	Titanium (TiAl6V4)	Stainless Steel (316L or 1.4404)
Density (g/cm ³)	2.68	4.41	7.9
Elongation at break (%)	Sep-13	13-15	25-55

Yield strength (MPa)	215-245	min. 860	380-560
Tensile strength (MPa)	335-355	min. 930	485-595
Tensile Modulus (GPa)	50-70	104-124	180
Hardness (HRB)	114-124	308-332	89

For the fatigue properties, in general, the material will higher fatigue is directly proportional to the smaller size of the powder used and the higher energy-density from the heat source [22].

3.2.3 Material from molten-based 3D printers

Similar to powder-based, Anisotropic also happens in the molten-based 3D printing. One explanation for the phenomenon is due to raster angle of the print. We provide a visualization of this angle in Figure 4. In general; the material will be stronger when loaded in the direction following its raster angle, compared to the other direction [23].

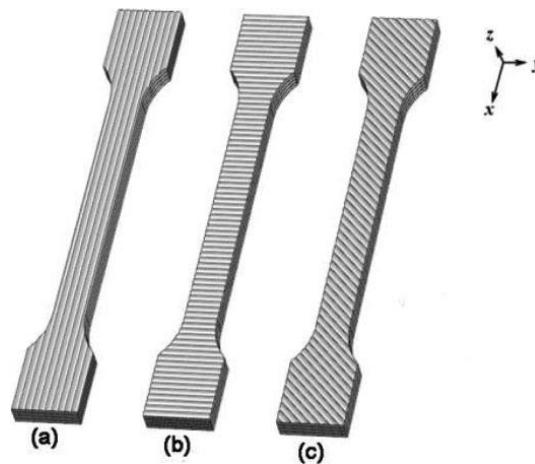


Figure 4. Anisotropy due to the raster angle of the specimens [32]

Another factor that can affect the mechanical properties of molten-based 3D printing materials is the air-gap between rasters. As can be seen in Figure 5, air gaps can form based on the raster of the printing. A positive gap (meaning the roads do not touch) can lead to stress concentration which then can lead to failure [24]. On the other hand, from the same publication, a negative gap (meaning the roads overlap, creating a denser part in that area) can result in higher tensile strength compared to zero gaps (meaning the roads are in contact with each other).

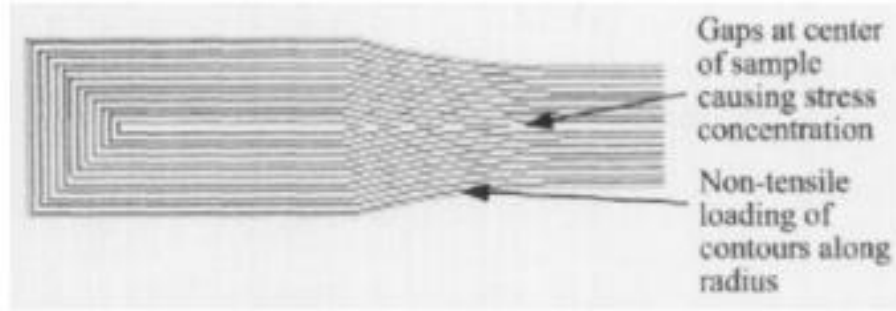


Figure 5. Air gap from a test specimen [30]

For the sake of comparison, we provide the summary of the mechanical properties of every common molten-based materials in Table vi Table vi. Summary of the mechanical properties of every common molten-based materials [31]. The data we use come from a compilation provided by one of a widely-used 3D printing slicer software [25]. We used this data due to the several additional information that is important for practical purposes they provide, most of which is usually missing from the academic literature

Table vi. Summary of the mechanical properties of every common molten-based materials [31]

	Molten-based material					
	ABS (Acrylonitrile Butadiene Styrene)	Flexible (Thermoplastic polyurethane)	PETG (Polyethylene Terephthalate Glycol)	PC (Polycarbonate)	PP (Polypropylene)	PLA (Polylactic Acid)
Density (g/cm ³)	1.04	1.19-1.23	1.23	1.2	0.9	1.24
Ultimate strength (MPa)	40	26-43	53	72	32	65
Stiffness*	5 out of 10	1 out of 10	5 out of 10	6 out of 10	4 out of 10	7.5 out of 10
Extruder Temperature (Celsius)	220-250	225-245	230-250	260-310	220-250	190-220
Maximum temperature before thermal deformation (Celsius)	98	60-42	73	121	100	52
Heated bed	required	optional	required	required	required	optional

*the Stiffness comparison is defined as “the difficulty to bend the material” in the source, as opposed to using the elastic modulus

For the fatigue data, generally, the literature has shown that a raster angle of 45° has a higher fatigue life [26,27]

3.3 Non-assembly mechanism

One of the key advantages of additive manufacturing is the possibility to design and realize a non-assembly mechanism. The non-assembly mechanism allows an engineer to fabricate a complex and functional structure regardless of any specialized manufacturing resources [28]. This feature, along with the high customizability of additive manufacturing process can result in a personalized “print and use” product for end customer. To achieve this means, an engineer can utilize either traditional-manufacturing-inspired rigid joint or compliance joint.

In a rigid joint, it usually consists of multiple bodies as a link and is restraining to only move in a specific Degree of Freedom (DoF). Figure 6 shows a range of example of rigid joints of various DoF. The clearance between parts plays a crucial role in ensuring the operationability of the joint. A clearance too big can cause joint vibration and instability while a clearance too small can cause an immovable joint [29]. As for now, this clearance value varies greatly to the additive manufacturing processes itself, and are highly experimental in nature to find the suitable setting for each process [28]. Additionally, support utilization (for additive manufacturing process from the molten-based processes) can also create issues as. Usually support removal can cause damage to the surface quality of the corresponding part. Moreover, apart from affecting surface quality, support generation can also hinder the mobility of the joint itself, as can be seen from Figure 7, while the removal of this support might be hard due to the small clearance from the parts.



Figure 6. A range of examples of rigid joints with various DoF [44]

In compliance joint, usually, the two to-be-connected parts are joined using a small structure(s) that can undergo a large deflection. As opposed to the rigid joint, non-assembly mechanism of compliance joint relies on the geometrical arrangement and the mechanical properties of involving material, on the contrary of relying on the geometrical accuracy of the part. Due to the involvement of large deflection, characterization of these kind of joint usually relies on a modeling approach due to the non-linear nature of large deflection, which is heavily affected by the geometrical design parameter of each type of joint [30]. We provide examples of several compliance joints in Figure 8

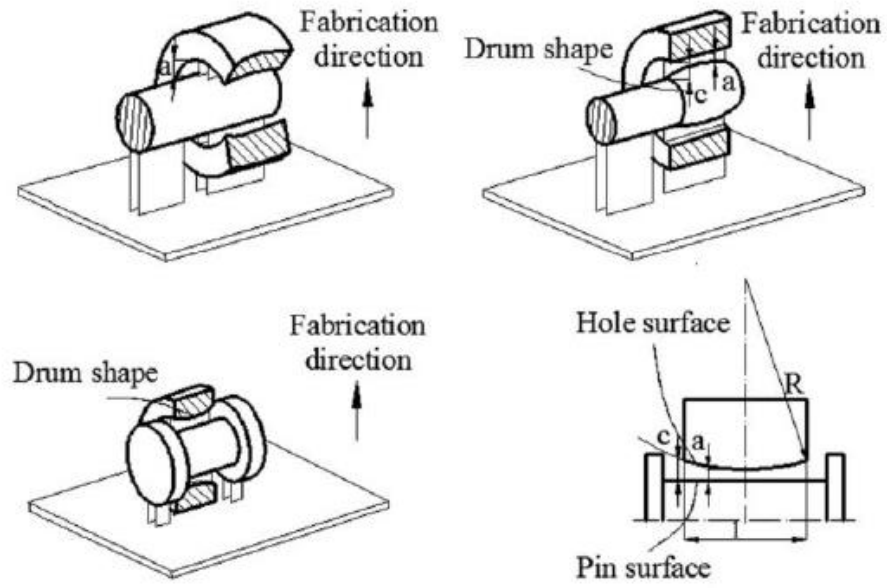


Figure 7. Support generation on a shaft-inside-a-hole hinders the mobility of the shaft itself [43].

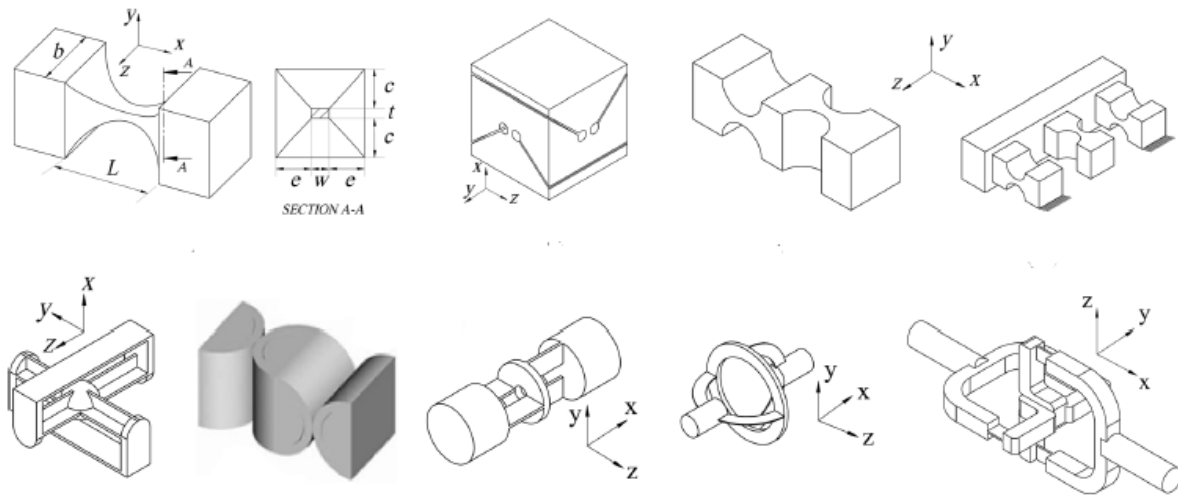


Figure 8. Examples of compliance joints [47].

3.4 Body-powered prosthesis basic user requirements

In this section, we will examine the general requirement of the design approach regarding a hand prosthesis. We will follow the requirement that Plettenburg has provided : control, cosmetics, and comfort [31].

3.3.1 Control

To control a transradial BP prosthesis, we can use a shoulder harness or elbow harness to generate the force for the cable. Shoulder harness has a higher movement variation compared to elbow harness but is harder to d-on and d-off [31]

Furthermore, the force from the cable is used to either close or open the prosthesis' grasp, depends on whether the prosthesis is voluntary-open (VO) or voluntary-closing (VC). In his publication, Sensinger reported that in general, VC's index of functionality is higher while also requires less force to operate (to close hand in VC or to open hand in VO) in comparison to VO [32]. Although he also stated that VO is preferred because it takes more effort to maintain the grasp in VC, locking mechanism directly addresses this particular problem.

Another thing to note is the hand opening width of the prosthesis, in which a certain value is desired to be able to grasp various objects. The Bowden cable's displacement will affect the value of the maximum hand opening value. While the exact relationship between the two depends greatly on the hand design, the locking mechanism should allow that displacement to take place. Smit and Plettenburg reported that the maximum value of cable displacement exhibited from several BP prosthesis is around 60mm [11]

While it is preferable to have a lower activation force because there is an influence of a high cable activation force on patient's ability to manipulate object [33], we will use the maximum amount of cable activation force from several BP (which is 131 N [11]) as the basis for the design of the locking mechanism.

3.3.2 Cosmesis

While the cosmetic value of a prosthesis arguably is a subjective matter that depends on each individual user, there are several design guidelines we can use. Firstly, a design featuring sharp edges should be avoided [30] because it can cause a tear to the cloth and can be painful if it touches the user's skin. Secondly, specific in developing countries, prosthesis users may want to look as normal as possible because people there might consider disabilities as some kind of bad stigma [13]

2.3.3 Comfort

Prosthesis's weight is considered to be the focal point of for user's comfortability on using a prosthesis [31]. Ideally, an addition of a locking mechanism should not alter the whole prosthesis system's weight. All of the aforementioned locking mechanism available in commercially are either installed in the socket (TRS, Inc. Sure-

Lock cable system) or in hand itself (APRL VC hand). In the latter case, the locking mechanism is included in the hand prosthesis itself. Thus we argue that the socket lock is better because it can be used as a generic locking mechanism for various other prosthetic hands.

Smit reported that a weight of 347 g is already considered as too heavy for an amputee with weak residual hand [34]. We will use this as a reference Cyborg beast hand's weight [7] for the weight of the socket in which the locking mechanism is installed.

3.3.4 Durability

A Prosthetist usually will perform a small maintenance for a prosthesis every 3-6 months [34]. Luchetti et al. reported that the minimum number of prosthesis's opening and closing cycle in one year is 75.000, with a median of 130.000 and a maximum of 790.000 [35]. We will use this data as a basis of the fatigue limit for the 3D printing material

3.5 Cable-Related Locking Mechanism from patent search

In this section, we review the variations of existing cable-related locking mechanism. We performed a patent review from *Espacenet.net* as the basis of the design of the locking mechanism. The search was conducted in the WW publication with these following terms: (1) Lock* AND prosthe* AND mechanism OR device, and (2) Lock* AND cable AND mechanism. The first search yields in 26 patents in English and the second search yields in 18 patents in English. After examining the resulting publications, we divided the locking mechanisms based on their locking principle and their locking interface. We show the complete findings in Table xi.

Differentiating by its principle, we distinguished the locking mechanism using shape lock and friction lock. In friction lock, the mechanism utilizes the contact friction between the cable and the brake pad from the mechanism. If the cable force exceeds the static friction generated by the mechanism, the cable will just "break free" from the lock. In shape lock, the locking mechanism will obstruct the cable's movement using an object that can be engaged or disengage to block cable movement's path. Should the cable force generate a strong enough stress, the obstructing object will break, and the mechanism will fail.

Differentiating by its interface, we distinguished the locking mechanism using 3 principles. The first principle is to lock the cable through an interface, exemplified by Figure 9. The locking mechanism afterward locks the interface in place, resulting in the locking of the cable itself. The second principle is to lock the cable directly, like in the left picture of Figure 10. In a force lock, the static friction happens between the brake and the cable itself directly, and in a shape lock, the obstruction is blocking the cable's path directly. The third principle is to lock the cable via mounting the cable in a winch, as can be seen in the right picture of Figure 10. If this which is restrained from a rotational movement, the cable can also be held in place via capstan equation. We summarize the classification of all locking mechanism found in the patent database in Table vii

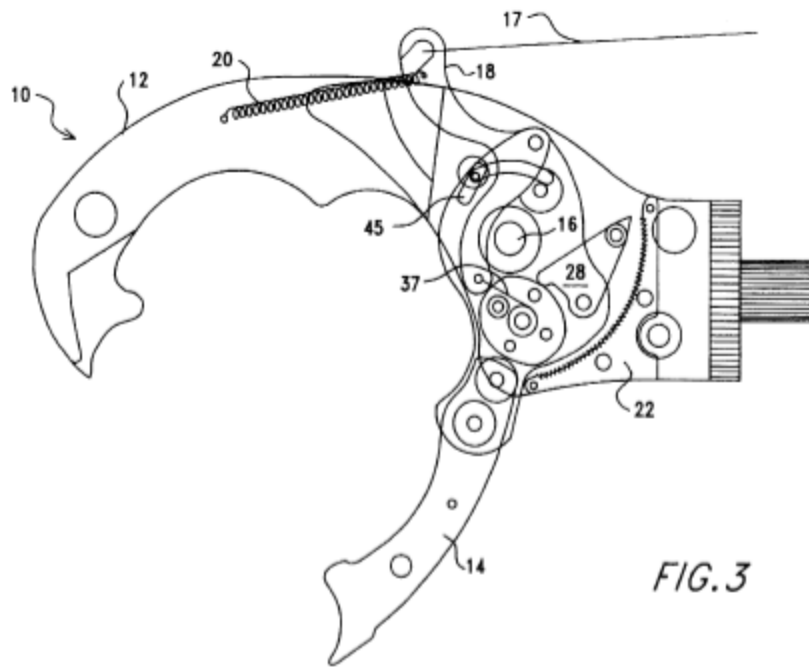


FIG. 3

Figure 9. Example of cable locked through an interface. Here the cable (17) is locked in its place via a pawl (28) and a ratchet (22) [43].

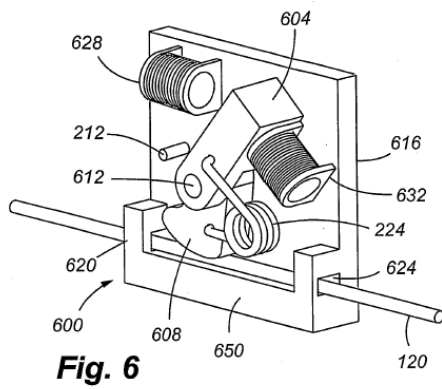


Fig. 6

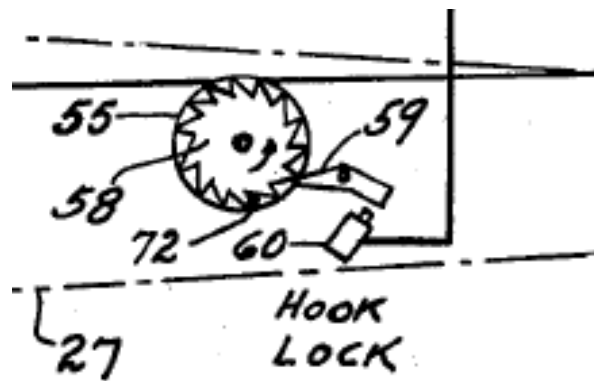


Figure 10 left: Locking the cable (120) directly with a cam 608 [44]; right: Locking the cable (72) via a winch (59) [45]

Table vii. Classifying our findings from the patent search

		Cable Interface			prosthesis locking mechanism (no cable)
		A (locked through an interface)	B (force acting directly on the cable)	C (cylindrical interface)	
Shape lock	engages lock manually	US2011140462, US6808407 (pin); US2004180568, US2009275246 (screw); US6447170 (snap-fit)	US2002184824 (electric motor)	US2006219144 (electric motor)	US5507837, WO9916391 (thread); US6626951, US2010094393, US4085506, US2010094393 (pin)
	engages lock automatically	US2002166351 (pin); US5800571 (ratchet)		US4074367 (ratchet)	US4795468, WO2006063363 (snapfit); US4074367, US2004030410, US200410285, US2016317327, US2005216096, US2005038522 (ratchet); US2012245707, US4659312, US2003195636, (spring +obstruction)
	Force lock		US2014048638 (electric motor); US2010132166, US2003046852 (hand); WO2006138388		US2017079810 (magnet); US2015202060 (vacuum); US6402789 (lever arm)
	permanent lock	US2018119725 (A1); US2017192190 (A1); US2018135780 (A1); US6354336 (B1)			US2009245554, US5935175, US7097663, US5468149
	Modified cable	US2018135780, US6354336			
	Unclear	US9876312, US6368141, US2001004851			US4650491

In several of the resulting patents containing shape lock, A ratchet was used. By adding ratchet, the locking device can engage independently from an input movement. This device, however, does not accommodate for an automatic disengagement, so an external input is still needed to release the lock.

3.6 Discussion

3.6.1 Process and material selection

As can be seen in Table II, FDM 3D printing machines certainly are the cheapest machine available in comparison from the machines from another process. In addition, FDM also has the highest number of machine variation compared to another type of 3D printing processes. We argue that the variation will increase FDM machines' accessibility to various developing countries in the world. Moreover, the filament cost for an FDM printer can be as low as 20\$ per Kg [36]. This price is much lower in comparison to the material cost from another process (e.g., SLA the cheapest of which is around 54 \$ per Kg [37] and SLS the cheapest of which is around 150\$ per Kg [38])

Among the material for FDM print, we chose PLA due to several reasons:

- PLA has the lowest melting temperature; thus, the 3D printing machine's extruder doesn't have to reach a high temperature, which might make the machine runs without relatively high power consumption.
- PLA doesn't require the machine to have a heated bed, making bed adhesion easier
- PLA has a relatively high strength compared to other common FDM material
- PLA is biodegradable

Jerez-Mesa et al. published a study regarding the fatigue lifespan of additively manufactured PLA parts [39]. In his study, he identified that the fatigue limit for bending stress of PLA is valued at approximately 45 MPa at 10k cycle within these conditions: (1) honeycomb infill with 75% density, (2) 0.5 mm nozzle diameter, (3) 0.3 mm layer height, and (4) printed perpendicularly of the shaft length, as can be seen in Figure 11.

Due to the anisotropic nature of FDM, the value of 45MPa is only valid to loading in any direction except along the z-axis (along with the build plate). There is no information regarding the fatigue limit on the z-axis direction from Jerez Meza's publication. To overcome this shortage, we will consider John Lee's publication regarding fatigue analysis of PLA [40]. In his publication, he performed a tensile test using an ISO 527 dog-bone in 3 different printing configurations (including z-axis direction). The ultimate tensile stress from the z-axis print valued approximately a third of the x-axis or the y-axis print. Thus, for loading calculation along the z-axis in this project, we will use a value of 15 MPa.

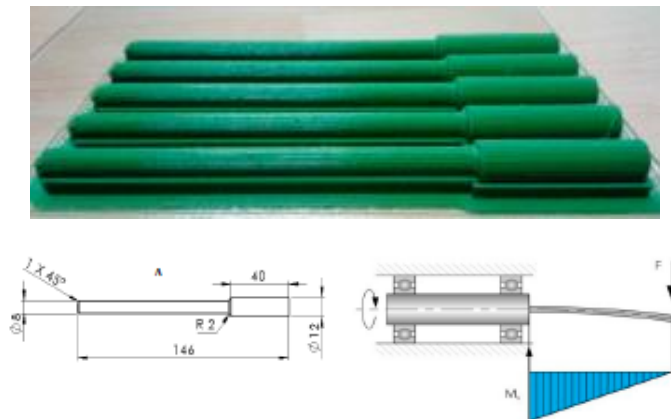


Figure 11. Print direction and the loading condition for identifying the fatigue limit of PLA [51]

3.6.2 Design constraint and design criteria

We defined design constraint and design criteria for the locking mechanism in Table VI and Table VII from the explanation in chapter 2.

Table VI. Design constraint for the locking mechanism

no	constrain	unit	
1	stress in x and y-axis*	MPa	45 MPa
2	stress in z-axis*	MPa	15 MPa
3	minimum dimension (smallest fabricatable dimension)	mm	0.5 mm
4	maximum dimension (boundary dimension)	mm	100x40x40
5	safety factor		1.5

* X and y axis are the direction normal to the build plate of the 3D printer's bed. Z axis is direction perpendicular to the build plate of the 3D printer

We propose constrain 1 and 2 based on the aforementioned fatigue limit of the PLA. Minimum allowed dimension is due to the common nozzle size of the common FDM machines. Maximum dimension is simulated to be 1 cm less compared to the average size of the thumb breadth and the hand thickness from Dutch 31-60 aged adult [dined 2004]. Lastly, the safety factor is proposed to be 1.5

Table VII. design criteria for the locking mechanism

critrion number	user's requirement	Technical problem	Must do (0)	Plan (1)	Wish (2)
1	control	Allowable force (N)	<410 N	410-600 N	>600 N
2	comfort	Weight (g)	50-30	30-10	<25g
3	cosmesis	Number of 'sticking out' edges	2	1	0
4	assembly	Number of assemblies required	2	1	0

In reality, the force of which the locking mechanism needs to overcome in order to lock the cable is the spring back force generated from the prosthetic hand's mechanism. This value depends greatly on the design of the prosthesis arm itself. For the arm used by the main hand prosthesis project governing this locking mechanism project, a non-linear behavior is expected between the pinch force generated vs. the shoulder's activation force.

As such, the maximum value of shoulder force (*Trapezius middle*) from Charlton's publication is used as the criteria [41].

While the commercially available 3D printed hands still rely on manual assembly, research around non-assembly hand has already begun since 2001 [42]. For this project, we aim for the locking mechanism to utilize additive manufacturing non-assembly mechanism so that the patient can immediately use the locking mechanism directly after printing.

For the weight, Ideally, the addition of the locking mechanism should alter the overall weight of the prosthesis system as little as possible. For this criterion, we use TRS Surelok's weight as the basis (50 g).

For the joints, we decided to use rigid joints, because compliance joints would require an engineer to spend more time finding the optimal to the geometry, which affects the mechanical properties directly. Another reason why we disregard compliance joint is because the characterization of PLA compliance joint is not understood to a degree of safe and reliable applications.

4

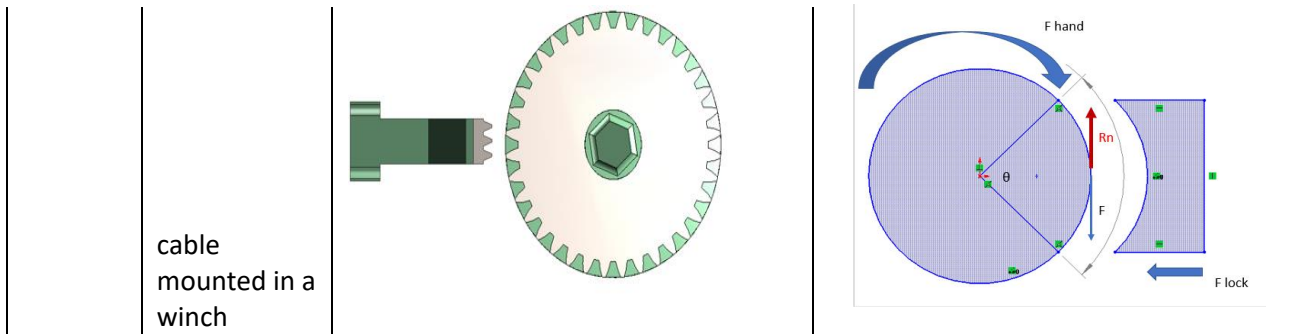
4. Design of the locking mechanism

4.1 Conceptual solution and winning concept

From the 6 categorizations of locking mechanism explained in chapter 3.5, we make 6 initial conceptual solution for the locking device which we show in Table viii

Table viii. Initial concept solution for the locking device

		Locking principle	
		Shape lock	Force lock
locking interface	Cable locked through an interface		
	cable locked directly		



4.2 Initial screening

For starter, we will disregard solution that mount the cable in an external interface. Our reasoning is that to use this interface, the cable needs to be split in two. Moreover, friction coefficient between PLA-PLA is lower (0.16 [46]) compared to nylon or steel cable to the aforementioned friction coefficient of nylon and steel (0.24 and 0.25 [47]).

Secondly, we will also disregard solution that uses force lock. Our reasoning is that force lock requires an active actuator which gives the system its load, generating normal force that is used to generate the friction force. No external actuator is utilized in a body-powered prosthesis, thus using force lock defeats the purpose of using a locking mechanism in the first place because the user still needs to provide the load actively.

Thirdly, we will also disregard the application of ratchet for our mechanism. Our reasoning is that ratchet operation needs a spring. At the moment, we do not have an extensive literature yet regarding a compliance PLA spring and its characterization in relation of its geometry.

Thus, we will examine further 2 concept solution, shape lock directly through the cable, and shape lock using a winch-mounted cable.

4.3 Shape lock directly through the cable

For this concept solution, we utilize a self-energizing brake. This concept applied moment generated by the spring force when the hand is coming back open as the friction force to lock the cable.

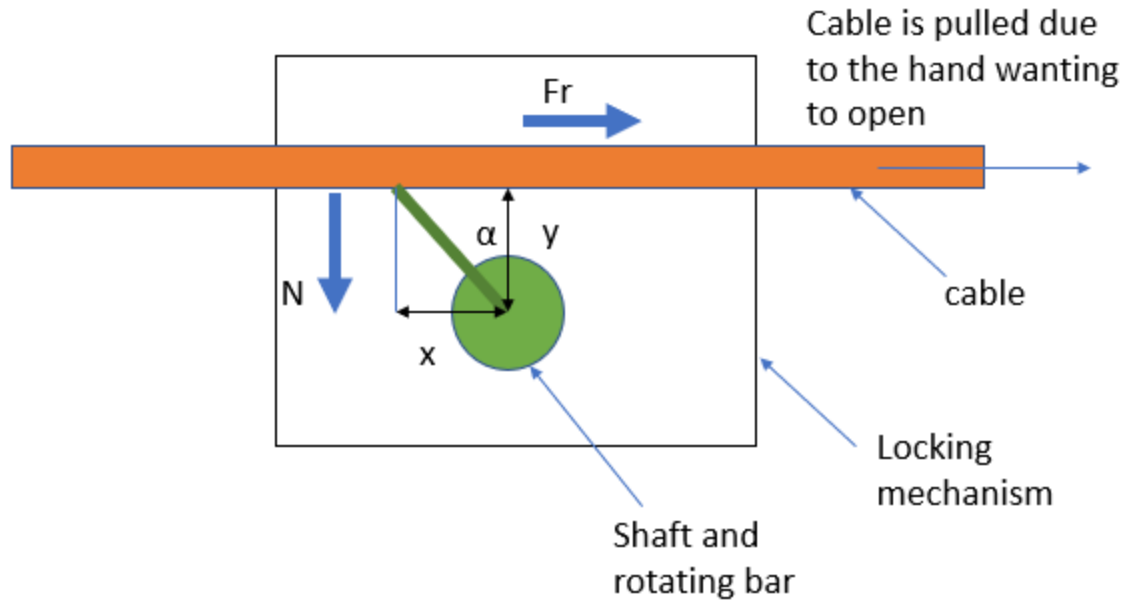


Figure 12. Self-energizing brake concept drawing. Here the force that happen due to the hand wanting to open is transmitted through the cable to the lock.

The calculation for the self-energizing condition is that

$$\curvearrow \text{Moment} > \curvearrow \text{Moment}$$

$$Nx < Fr y \mu$$

Because $Fr = N$, we have

$$x < y \mu$$

$$\mu > \frac{x}{y}$$

$$\mu > \tan \alpha$$

Where

$$Fr = \text{Hand force}$$

$$N = \text{Normal force due to the hand force}$$

$$\mu = \text{coefficient of friction}$$

In theory, following this scheme, the cable can be locked with force applied through the Hand force as much as the material allowed. For that reason, we will examine the beam equation for the green locking bar

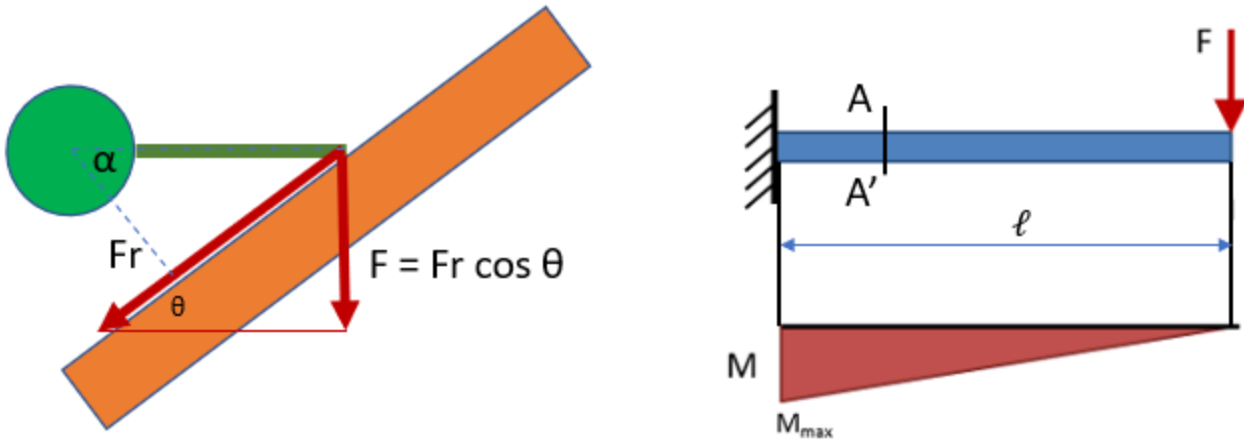


Figure 13. Beam equation for the locking bar. The force acting on the beam is the cosine of the hand force due to the locking bar start to lock at a certain angle, not all the way at 90 degree

By trigonometry, we will have $\theta = 90 - \alpha$. Thus, we have

$$F = Fr \cos \theta$$

The maximum bending stress experienced on a beam is defined as

$$\sigma_{\text{bending}} = \frac{M_{\text{max}} \cdot y}{I}$$

Where

$$M_{\text{Max}} = F \cdot \ell$$

With

y = the distance of the cross sectionn's neutral axis to the furthest point of the crosssection

I = the second moment of inertia of corresponding (A – A') cross – section

ℓ = length of the bar

From this initial calculation, we propose the design a proof of concept for this mechanism in Figure 14.

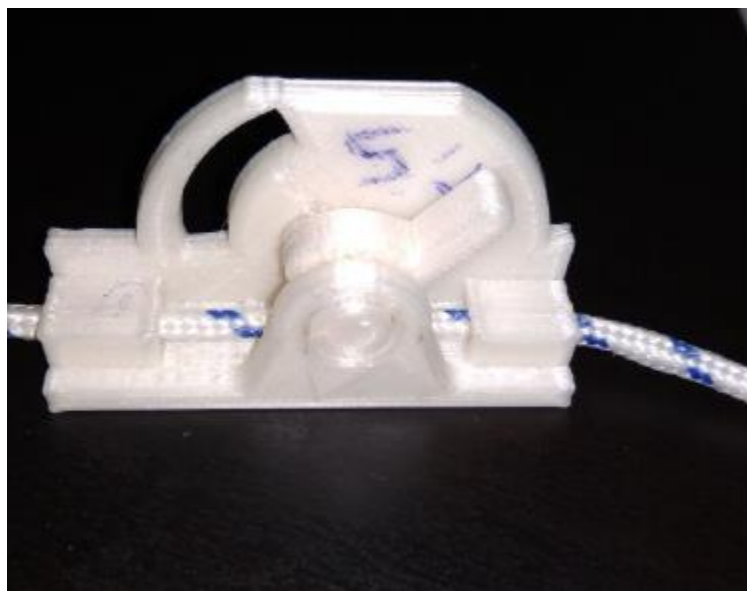
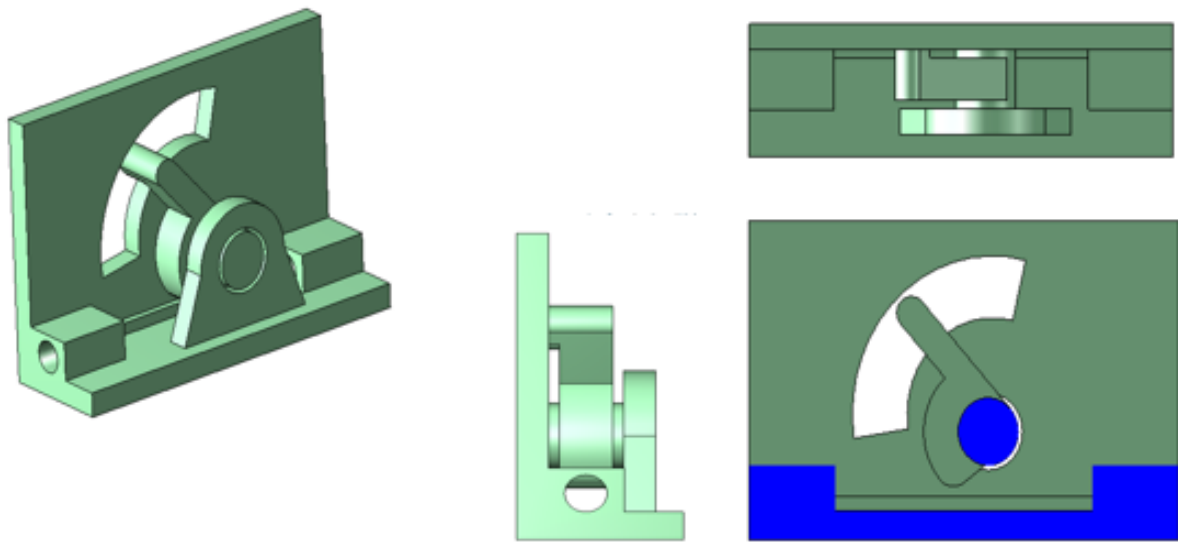


Figure 14. Global CAD for the self-energizing and the realization of the concept

We use quarter circle as a replacement for the green bar from the previous calculation because this geometry allows the thickness of the bar to be maximum in the place where the maximum bending moment happens

In that case, we use the second moment of inertia of:

$$I \text{ of } x - \text{axis} = \frac{b \cdot h^3}{3}$$

We will set b to be similar to the diameter of the cable used. The stress calculation for this mechanism is:

$$\sigma_{\max} = \frac{M_{\max} \cdot y}{I}$$

$$\sigma_{\text{bending}} = \frac{F_{\max} \cdot \ell \cdot r}{\frac{1}{3}bh^3}$$

Because ℓ , r , y , and h are set to be equal, we have:

$$\sigma_{\text{bending}} = \frac{F_{\max} \cdot r \cdot r}{\frac{1}{3}br^3}$$

For nylon cable:

$$4.5 \cdot 10^6 \frac{1}{\text{safety factor}} = \frac{F_{\max} \cdot r \cdot r}{\frac{1}{3}3 \cdot r^3}$$

$$F_{\max} = 3 \cdot 10^6 \cdot r$$

We present a table for a couple of possible configurations using different value of r

Table ix. Possible configurations using different value of r for the radius of the locking bar

y	x	$y^2 + x^2$	r	F max given sigma max	
				F nylon (kN)	F hand nylon (kN)
2.00	0.50	4.25	2.06	6.18	6.44
3.00	0.75	9.56	3.09	9.28	9.66
4.00	1.00	17.00	4.12	12.37	12.88
5.00	1.25	26.56	5.15	15.46	16.11
6.00	1.50	38.25	6.18	18.55	19.33
7.00	1.75	52.06	7.22	21.65	22.55
8.00	2.00	68.00	8.25	24.74	25.77
9.00	2.25	86.06	9.28	27.83	28.99
10.00	2.50	106.25	10.31	30.92	32.21
11.00	2.75	128.56	11.34	34.02	35.43
12.00	3.00	153.00	12.37	37.11	38.65
13.00	3.25	179.56	13.40	40.20	41.88
....					
18.50	4.63	363.64	19.07	57.21	59.59

As we can see, the maximum force this configuration can withstand increases as the radius of the locking bar increase. The maximum possible force in relation to the maximum dimension (a radius of 19) is around 60 KN for nylon cable and 30 KN for steel cable

Another critical area we will examine is the shaft containing the locking bar.

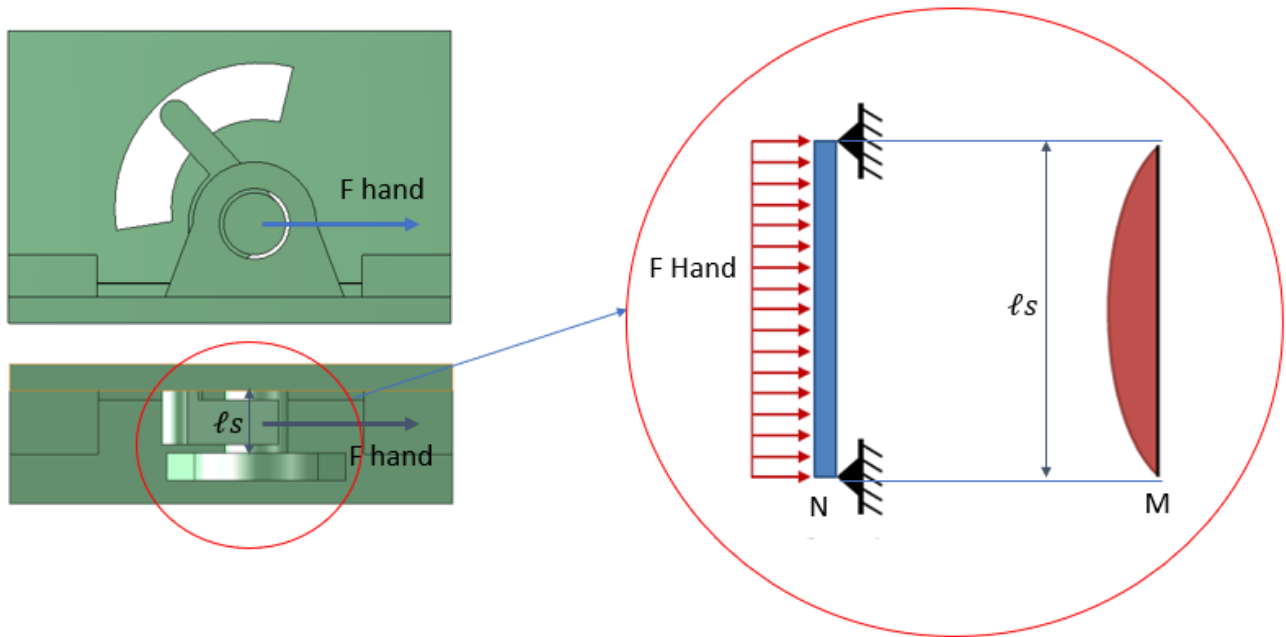


Figure 15. Stress analysis in the shaft area

Where L is the diameter of the cable and l_s is the length of the shaft. The maximum bending stress for this region is :

$$\sigma_{\max} = \frac{M_{\max} \cdot y}{I}$$

In this configuration, the maximum moment is :

$$M_{\max} = \frac{F l_s^2}{8}$$

And the second moment of inertia is:

$$I = \frac{\pi}{2} r^4$$

Thus, we have:

$$\sigma_{\max} = \frac{\frac{F l_s^2}{8} \cdot r}{\frac{\pi}{2} r^4}$$

$$1.5 \cdot 10^6 \cdot \frac{1}{\text{safety factor}} = \frac{F_{\max} l_s^2 \cdot r}{8 \cdot \frac{\pi}{2} r^4}$$

We present a table for the resulting force using a different possible value of r

Table x. Possible configurations using a different value of r for the shaft

r (mm)	F max (kN)	F max (kN)
0.50	0.17	0.70
1.00	1.40	5.58
1.50	4.71	18.84
2.00	11.16	44.66
2.50	21.81	87.22
3.00	37.68	150.72
3.50	59.83	239.34

The maximum possible force at the radius of 19 is 9 Giga Newton for nylon cable.

This conceptual solution can be printed with no assembly. The weight of this mechanism is approximately two grams at r locking bar = 7 mm and r shaft = 5mm

4.4 Shape lock using a cable that is mounted in a winch

In this solution, the capstan equation is the main governing equation. This equation deals with the amount of force a capstan can hold an installed rope to be stationary should that rope is to be subjected to a force.

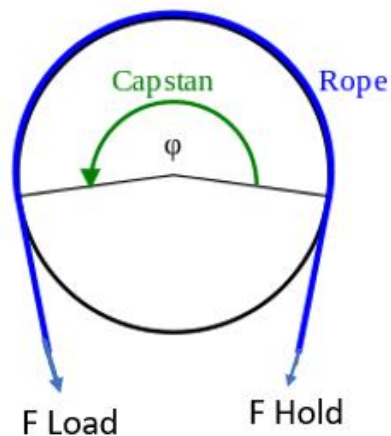


Figure 16. Force analysis in a capstan device

$$F_{\text{load}} = F_{\text{hold}} \cdot e^{\mu\theta}$$

Where

μ = friction of PLA and nylon

θ = rope contact angle(in radians)

We can see that as the number of wrapping from the rope increase, the Load that the capstan can also hold increases. For the wrapping and the winch configuration, we will follow the configuration from the study Gemmell et al. conducted [10]. He informed that there has to be a fillet presents with the value of $1.5 \times$ the cable's diameter in order to avoid cable overwrapping each other at the end of the winch. As such this results in the maximum diameter value of 14.5 mm

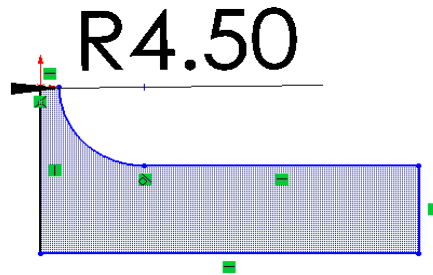


Figure 17. Optimal design for the end part of the winch

Table xi

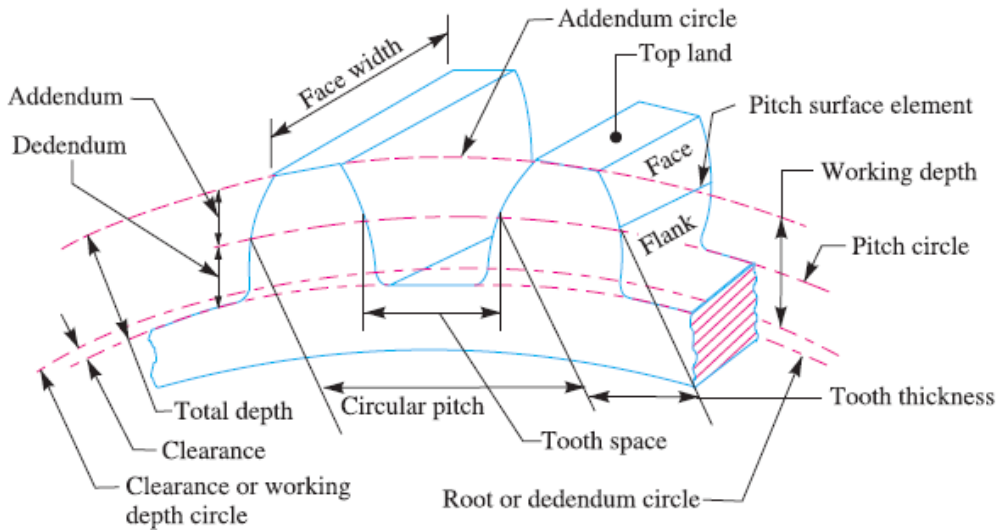


Figure 18. Anatomy and term used in gears

Table xi. Gear specifications utilized with the reasons

	type	reasoning
teeth form	involute	Not prone to error due to geometric inaccuracy, more commonly used
Gear teeth system	20° full depth	Highest tooth strength
module	1	Lowest standardized module. Lower module -> shorter tooth -> more strength

For the strength limit, Lewis Equation is used:

$$F_{\max} = \sigma_{\max} \cdot pc \cdot \text{gear width} \cdot Y$$

Where Y is the Lewis form factor which value is

$$Y = 0.154 - \frac{0.912}{\text{Number of teeth}}$$

And pitch circle (pc) is

$$pc = \frac{\pi}{\text{Module}}$$

We will disregard velocity factor due to the operation velocity being at 0 ms⁻². Because we have a module of 1, we can design the full gear anatomy using a standard proportion of gear system. Following the standard in Figure 3.4.3.2, the module value of 1, and the value of maximum addendum circle of 39mm (1mm less of the maximum dimension allowed) , yields in the number of tooth as 37.

S. No.	Particulars	14½° composite or full depth involute system	20° full depth involute system	20° stub involute system
1.	Addendum	1 m	1 m	0.8 m
2.	Dedendum	1.25 m	1.25 m	1 m
3.	Working depth	2 m	2 m	1.60 m
4.	Minimum total depth	2.25 m	2.25 m	1.80 m
5.	Tooth thickness	1.5708 m	1.5708 m	1.5708 m
6.	Minimum clearance	0.25 m	0.25 m	0.2 m
7.	Fillet radius at root	0.4 m	0.4 m	0.4 m

Figure 19. Table of standard gear proportion [48]

Thus the maximum allowable force with the relation of the gear's width is:

$$F_{\max} = 3 \cdot 10^6 \cdot \frac{\pi}{1} \cdot \text{gear width} \cdot 0.154 - \frac{0.912}{37}$$

Table xii. T

gear width	Max allowable force (N)
1	609.54
2	1219.07
3	1828.61
4	2438.14
5	3047.68
6	3657.22
..	
12	7314.43

From this initial calculation, we propose two conceptual solutions. The first conceptual solution is mounting the winch via applying Emmet Lalish's gear bearing [49] as a mean to 3D print preassembled rotating part. This gear bearing is designed through a parametric process which generates the entire geometry with an input of the outer diameter. The second conceptual solution is mounting the winch without the gear bearing.

4.4.1 With Gear Bearing

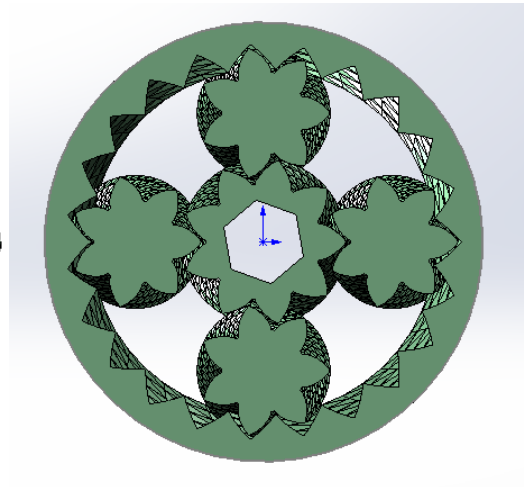
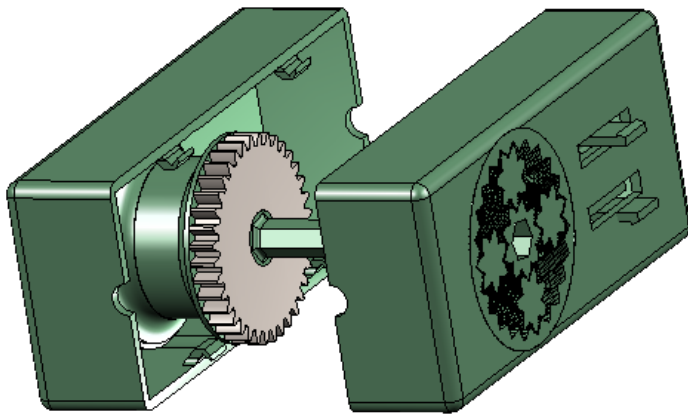


Figure 20. Left: Global Cad for the gear bearing. Right:

gear bearing.

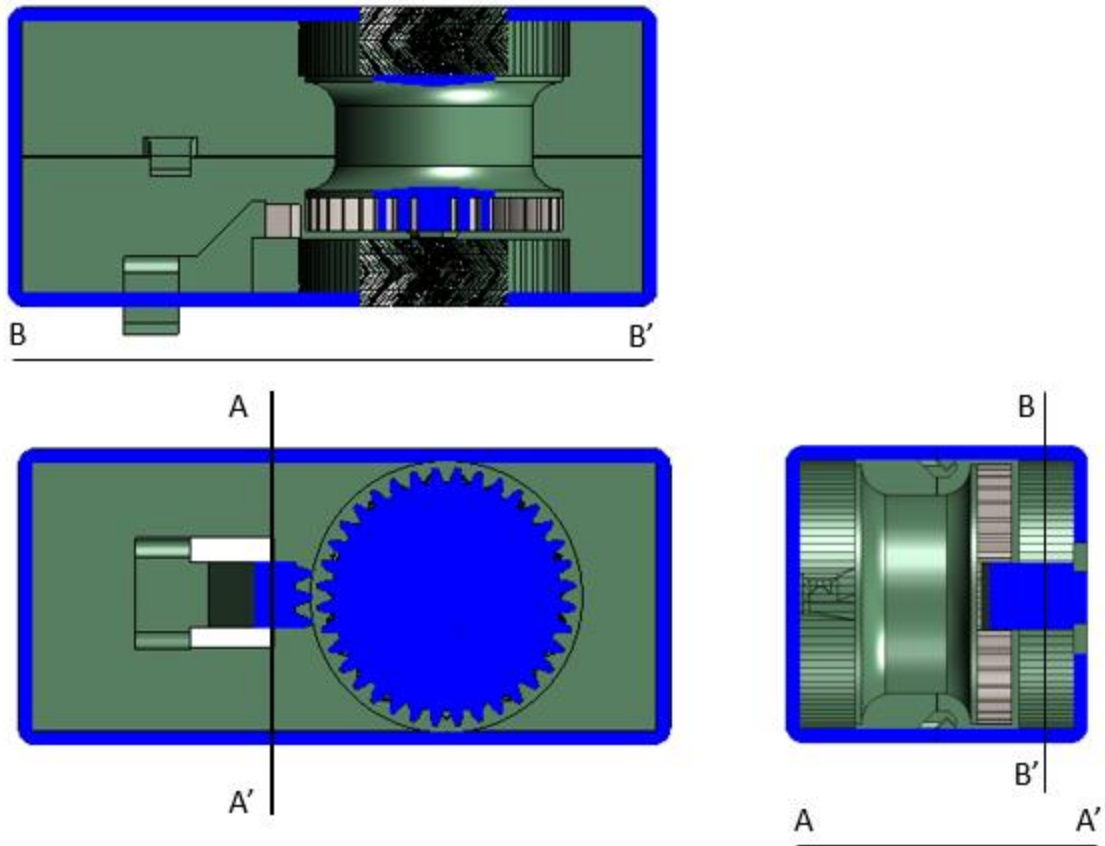


Figure 21. Orientation view for the global CAD

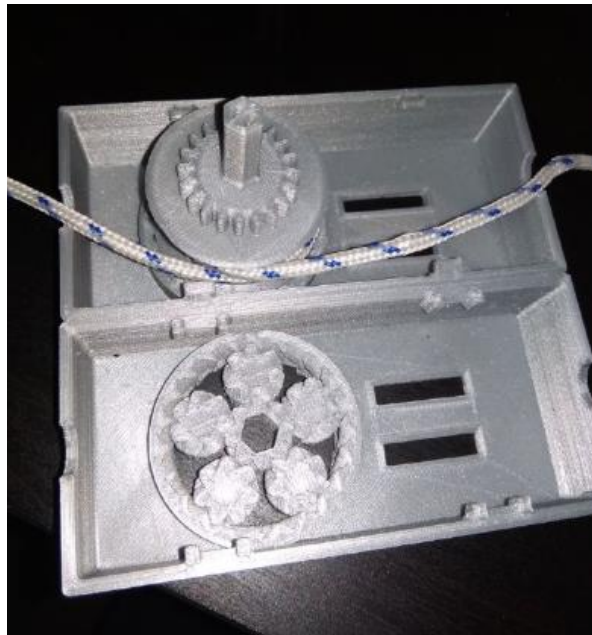


Figure 22. Realization of the concept

For the stress calculation, we identified the critical component which is the hexagonal connector between central sun gear in gear bearing on the right body in the figure and the winch.

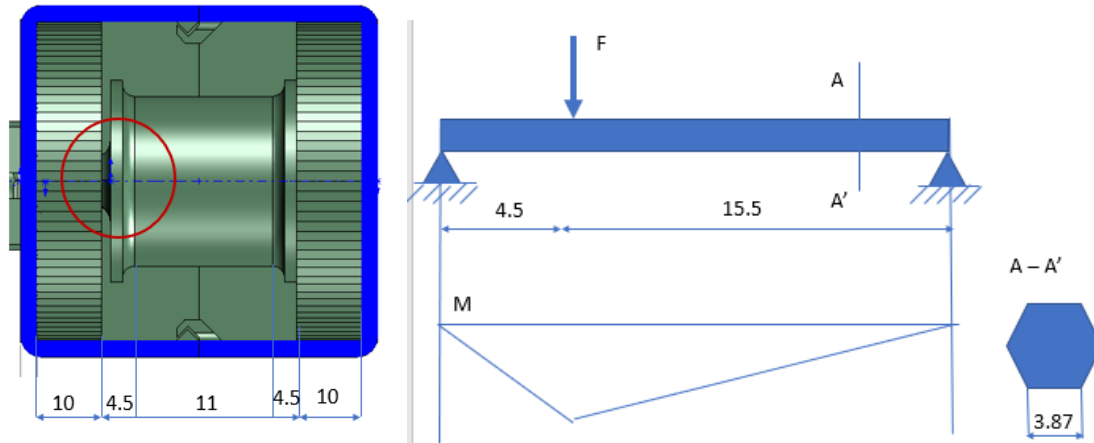


Figure 23. Critical components for the winch

The maximum moment is

$$M_{\max} = \frac{4.5 \text{ mm } 15 \text{ mm}}{20 \text{ mm}} F_{\max}$$

And the inertia of hexagon is

$$I = \frac{5\sqrt{3}}{16} a^4$$

Where a is 3.87 in this case. Thus, the max force allowed is

$$1.5 \cdot 10^6 \cdot \frac{1}{\text{safety factor}} = \frac{\frac{4.5 \text{ mm } 15.5 \text{ mm}}{20 \text{ mm}} F_{\max} 3.87 \text{ mm}}{\frac{5\sqrt{3}}{16} (3.87 \text{ mm})^4}$$

$$F_{\max} = 13.5 \text{ N}$$

This concept needs minimal 1 assembly because the left and right body in Figure 3.4.3.1a needs to be separated to enable cable installation. The Weight of this concept is 26 gram.

4.4.2 Without gear bearing

In this concept, we discarded the gear bearing to achieve stronger shaft with the tradeoff of lowering the efficiency of the device while the winch is rotating.

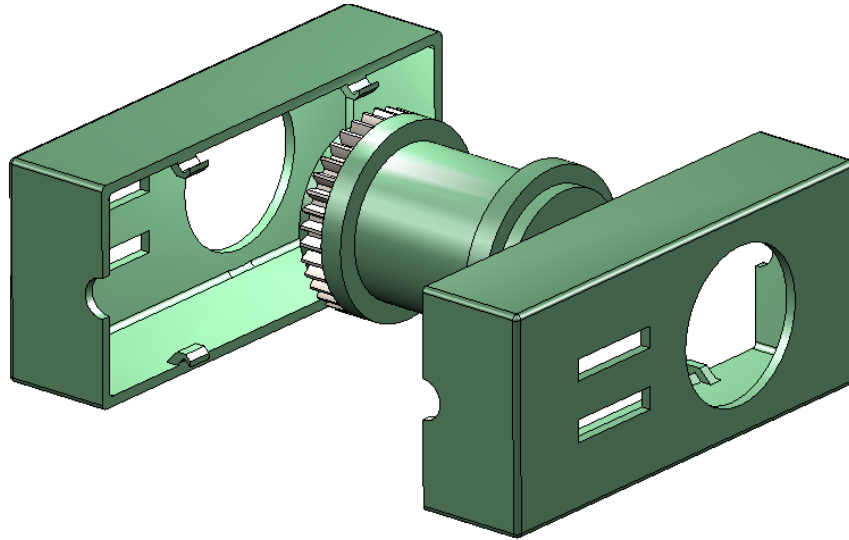


Figure 24. Exploded view of the solution without bearing

The stress calculation is similar with the exception of some geometrical arrangements and the cross-section that is used for the inertia calculation (which is now the diameter of the winch itself).

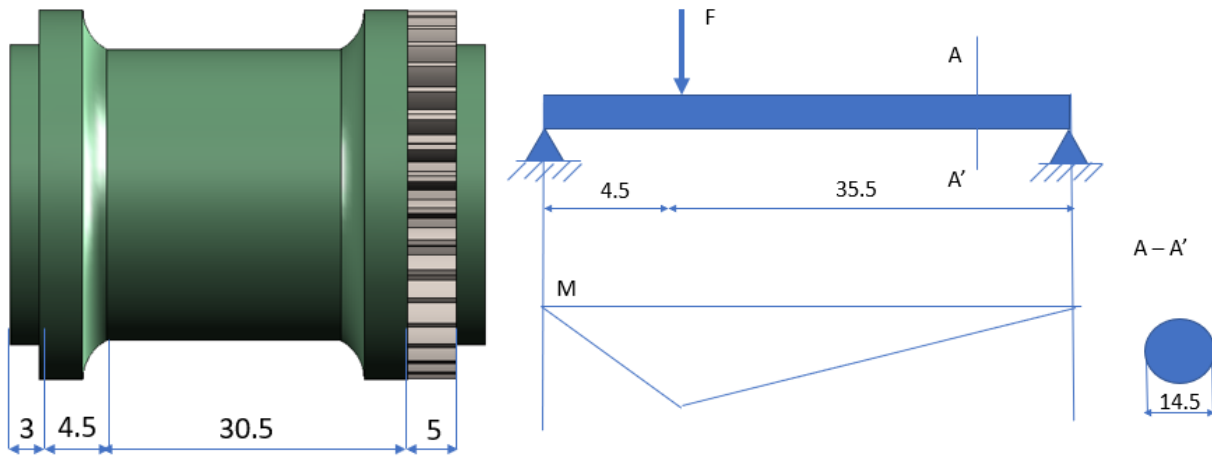


Figure 25. Critical components for the winch without the gear bearing

The maximum moment is

$$M_{\max} = \frac{4.5 \text{ mm } 35.5 \text{ mm}}{40 \text{ mm}} F_{\max}$$

And the inertia of circle is

$$I = \frac{\pi}{2} r^4$$

Where a is 3.87 in this case. Thus, the max force allowed is

$$\sigma_{\max} = \frac{M_{\max} \cdot y}{I}$$

$$1.5 \cdot 10^6 \cdot \frac{1}{\text{safety factor}} = \frac{\frac{4.5 \text{ mm} \cdot 35.5 \text{ mm}}{40 \text{ mm}} F_{\max} \cdot 14.5 \text{ mm}}{\frac{\pi}{2} (14.5 \text{ mm})^4}$$

$$F_{\max} = 485.21 \text{ N}$$

Because the winch is printed separately, this concept needs an additional assembly compared to solution featuring gear bearing. The weight of this assembly is 17 g

4.5 Discussion

The utilization of the gear bearing gives the shaft and the enclosure to be printed in 1 go. Despite that, this concept still needs assembly in order to install the cable because installing the cable from outside is not possible. A huge tradeoff, however, is that the diameter of the shaft cannot be high due to the design of the bearing. Moreover, due to the printing of the shaft being on top of the bearing, the stress that the part will be experienced comes in the shearing direction of the print which also lessens the maximum force it can withhold.

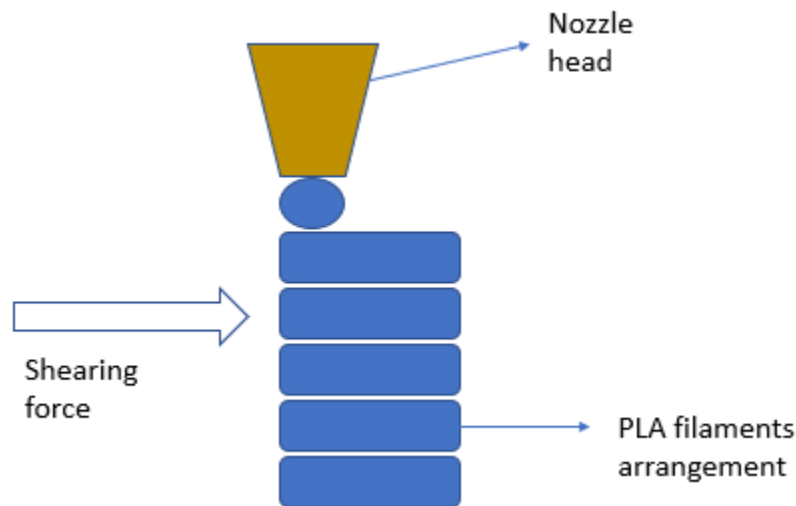


Figure 26. The shear force experienced in the shaft

On the contrary in the gearless solution, the minimum value of the shaft's diameter in the critical area can be as big as the diameter of the shaft itself as can be seen in Figure 25. Even though the shaft still cannot be printed in the xy direction due to the existence of the gear teeth, an increase of diameter will contribute greatly to the strength because they have an exponential relationship.

In the case of the self-energizing solution, the critical components are the shaft that hosts the locking bar and the locking bar itself that withstand the cable force and turns it into normal force for the lock. Both of this critical component has bigger freedom in its size in comparison to the critical component from the winch solution, as can be seen in Table ix and Table x. In an exaggerated way, the size of the shaft and the locking bar can be as big as the maximum dimension allowed. Despite that, using a relatively small value of r can already fulfill the allowable force criterion. Moreover, using appropriate clearance, the self-energizing can be printed with no assembly between the locking bar and the rest of the part.

4.5.1 Selection Winning Concept

We provide a comparison of the 3 solutions in relation to our design criteria in Table xiii

Table xiii. Design criteria of the 3 solutions.

	Allowable force (N)		weight (g)		sharp edges (#)		Assembly required		Total score
	value	score	value	score	value	score	value	score	
<i>Requirement</i>	410	0	50 - 30	0	2	0	2	0	
<i>Plan</i>	410 - 600	1	30 - 10	1	1	1	1	1	
<i>Target</i>	>600	2	<10	2	0	2	0	2	
Self-energizing	>600 (up until 28KN)	2	Can be as low as 2	2	No sharp edges	2	0	2	8
Winch with gear bearing	13.5	0	26	1	No sharp edges	2	1	1	4
Winch without gear bearing	485	1	17	1	No sharp edges	2	2	0	4

As we can see the concept using self-energizing is superior in term of allowable force, weight, and assembly requirement. As such, we will choose this concept solution moving forwards.

4.5.2 Assessing the Critical Components from the self-energizing solution

In the self-energizing concept, the physical relationship between components inside the locking mechanism and their interaction with outside components will be presented in Figure 27 with the functional flow (in the form of mechanical force) presented in Figure 28. From these components, there are 3 critical elements that made the locking mechanism functional; the rotatable locking bar, the cable, and the locking surface. In our concept

example in chapter 4.4.2, the rotatable locking bar is combined with an operating lever as a component that the user can use to engage the lock. The other component is the frame which holds the locking bar and the locking surface. From the explanation in chapter 4.4.2, in the calculation, we know that the critical aspect of this locking mechanism lies in the surface friction between the wire and both the locking bar and the locking surface. We present the part-to-part relationship and the functional flow of this conceptual solution in Figure 27 and Figure 28

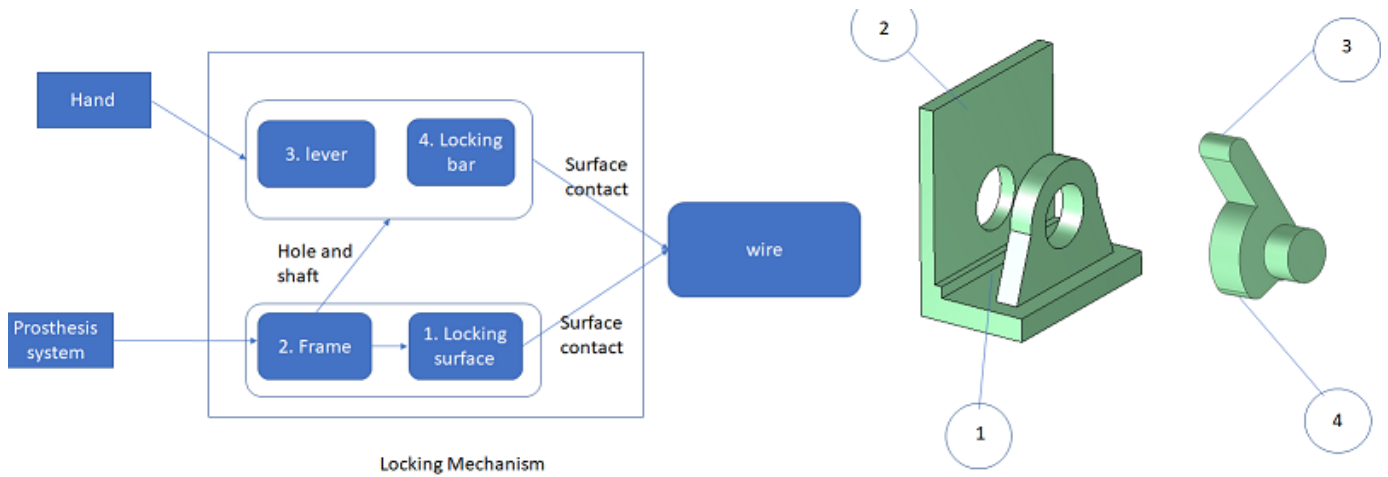


Figure 27. Part-to-part relationship in the locking mechanism

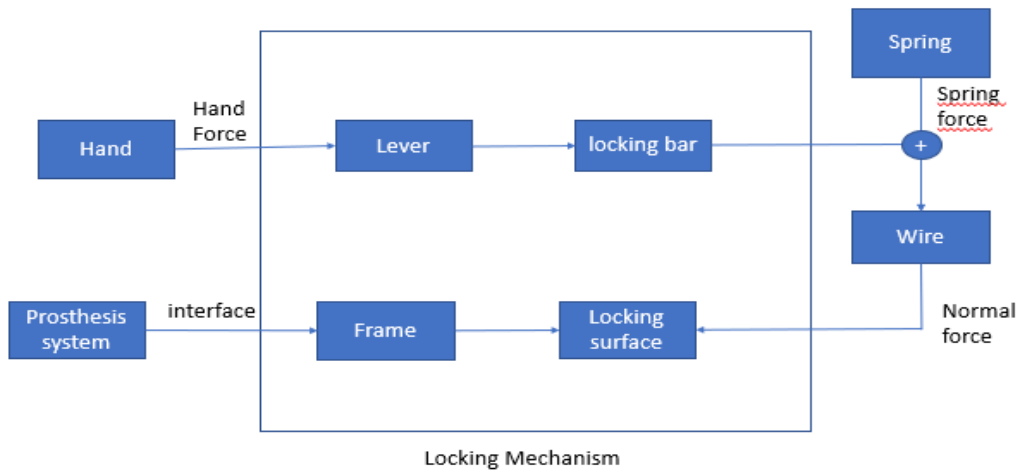


Figure 28. Functional flow in the form of mechanical force

We will optimize the locking bar and the locking surface in order to achieve maximum performance, which we will show in Chapter 5. In Chapter 6, we will design the frame and the lever along with the incorporation of the locking bar and the locking surface to produce the complete prototype.

5

5. Optimization of the Locking mechanism

In this chapter, we will evaluate several printing parameters and design variations that could contribute to a difference in the performance of the locking mechanism.

5.1 Methodology

To assess the performance of a locking mechanism, we use a test bench which is a modified version from the pinch force test bench used in Gerwin Smit's publication [11]. In this version, the cable will be mounted between an actuator spindle and a bar load cell, connected through a tension springs of various constants. The load cell is connected through an amplifier to an Arduino system. The locking mechanism is installed between the spindle and the spring. We present the schematic drawing, the components specification table, and the actual picture of the test bench in Figure 29, Table xiv and Figure 30 respectively. The tension springs are used to simulate hand prostheses of which their constant resembles various prostheses system Gerwin characterized in his publication [11]. In the end, we chose springs with constants of 1.1 N/mm and 1.7 N/mm. After installing the locking mechanism, we pull the spring with the spindle manually up to give force to the load cell. Afterwards, we engage the lock and turn back the spindle to the original location to relieve the tension on the cable to the right side of the locking mechanism. Lastly, we record the force retained by the load cell afterward to simulate the pinch force drop from the prosthesis. All of the specimens were printed using a printer with 0.4 mm nozzle size.

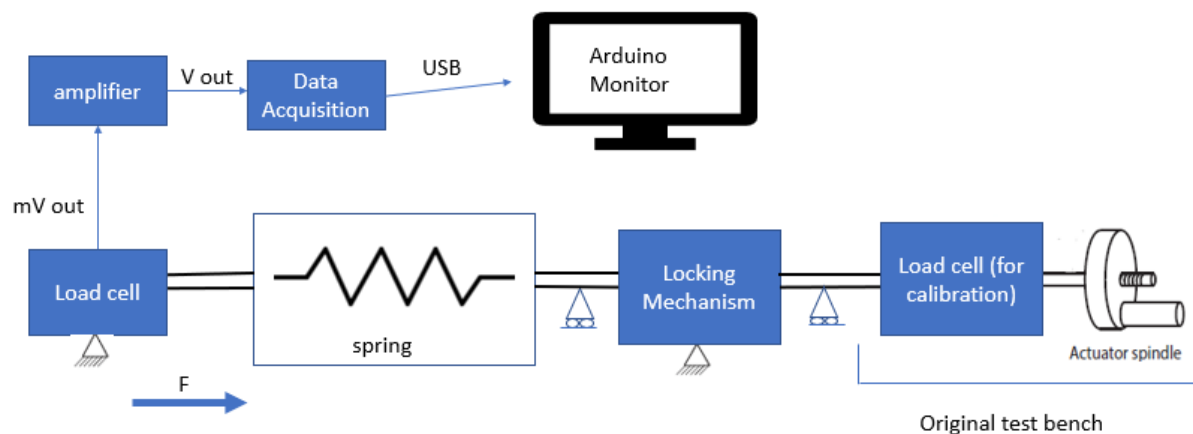


Figure 29. Schematic overview of the test bench

Table xiv. Components of the test bench

	Components	Description
1	Load Cell	Straight bar 10kg TAL220
2	Amplifier	Load cell amplifier HX711
3	Data Acquisitor	Arduino based Redboard

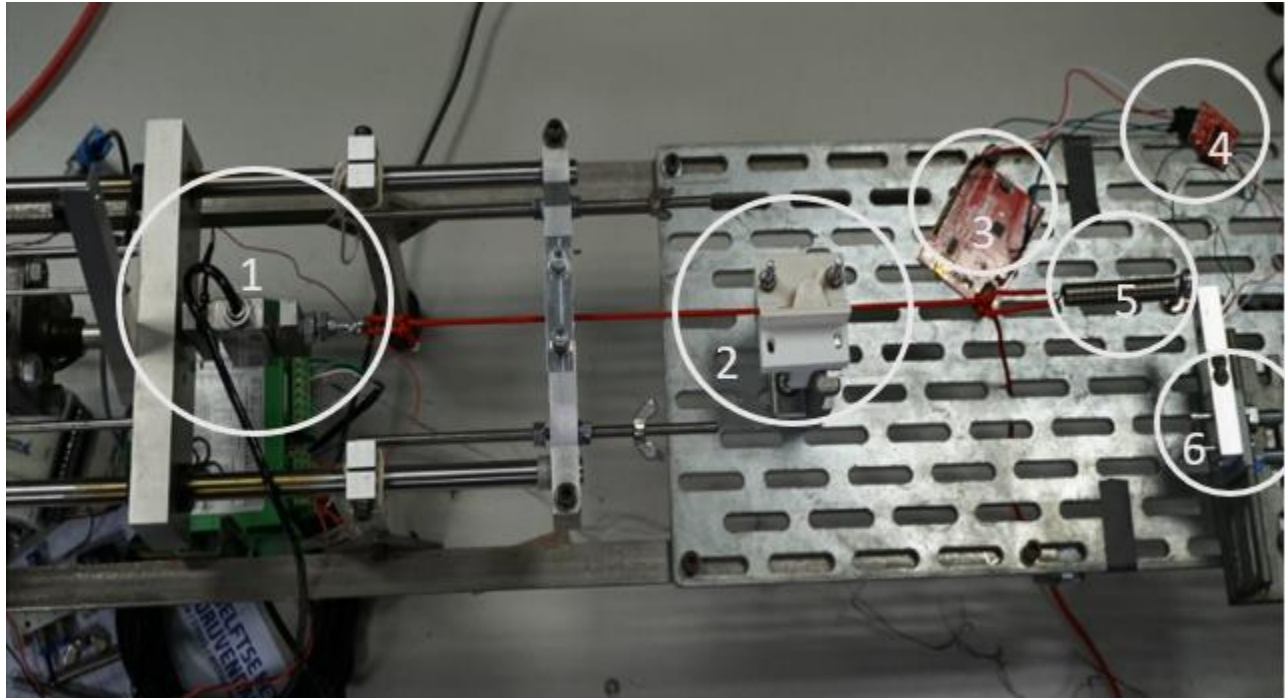


Figure 30. Actual picture of the test bench; (1) Load cell (for calibration), (2) Locking mechanism sample, (3) Redboard, (4) Load cell driver, (5) spring, (6) load cell

5.2 Result

5.2.1 The effect of the build direction

It is important to consider the build direction in additive manufacturing because it affects the material properties, along with the surface finish and the accuracy of the parts. In this case, we will test two build direction of the locking mechanism, vertical build where the shaft and the hole will be printed vertically, and horizontal build where the shaft and the hole will be printed horizontally. Figure 31 shows the build process for each build on a slicer software. The finished product can be seen in Figure 32. Afterwards, we pull these specimens with 20 N of force and engage the lock. Lastly, we release the activation force and then record the amount of force these specimens can retain. We show the result of this measurement in Table xv.

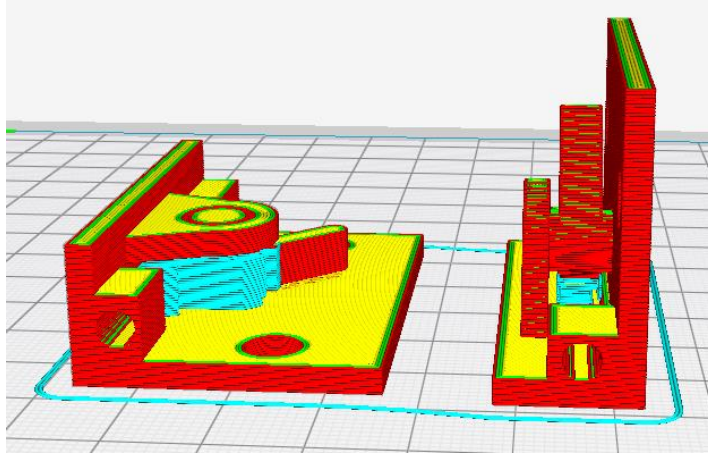


Figure 31. Part display for two different build orientation in the slicer software. Left is for vertical build, and right for horizontal build.

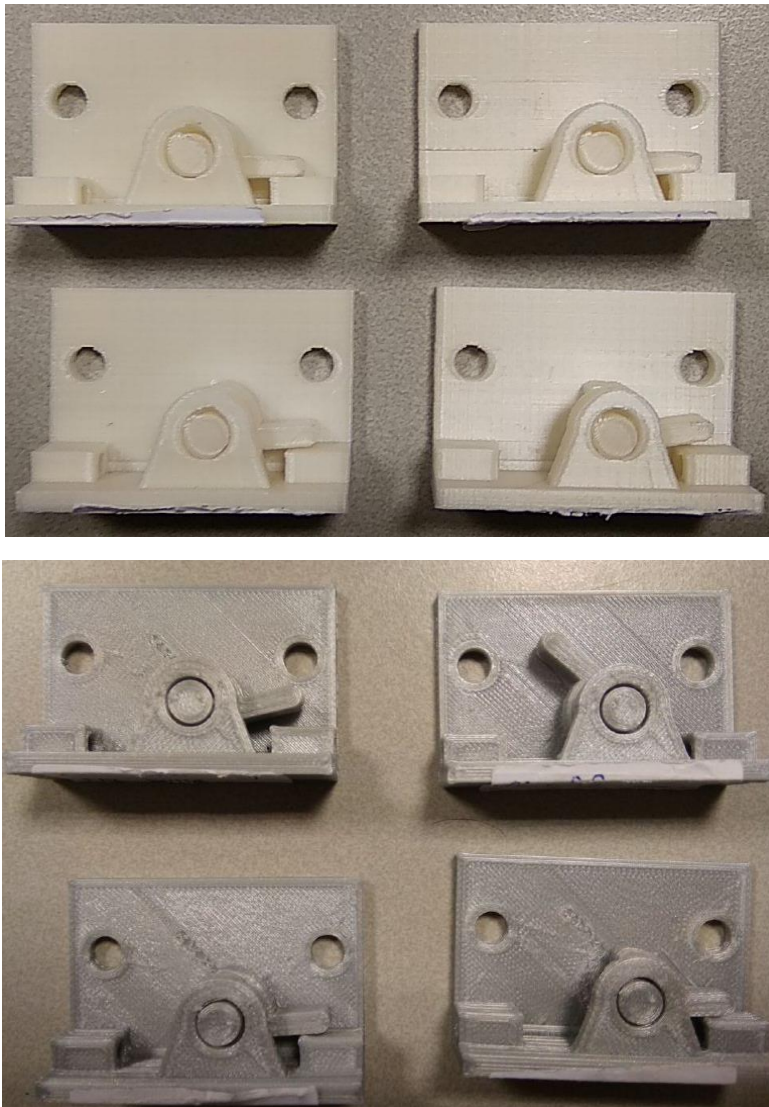


Figure 32. Printing result for two different build direction. Specimens on the top picture were horizontally build and specimen on the bottom were vertically build

Table xv. Measurement result for vertical build and horizontal build specimens pulled to 20N of spring force

		Spring coefficient	
		1.1 N/mm	1.3 N/mm
Horizontal Build	sample 1	12	15.3
	sample 2	18.4	17.6
	sample 3	16.8	17
	sample 4	16.7	16.8
	mean	15.98	16.68
	Stdev.	2.76	0.98
Vertical Build	sample 1	17.7	17.7
	sample 2	18.8	18.4
	sample 3	19.1	18.1
	sample 4	18.3	18
	mean	18.48	18.05
	Stdev.	0.61	0.29

Per Table xv, we can see that the precision of the vertical build specimens are higher in comparison to the precision off the horizontal build specimens due to the standard deviation.

5.2.3 The effect of surface topology on the performance.

In this section, we tried to apply several sizes of topology modification for increasing surface friction featured in Petterson’s study [50]. In the study, Petterson found that an array of triangles with a point degree of 70.5° will achieve maximum surface friction. We tried to use the array with several clearances. The clearance used is the multiplication of the nozzle diameter of the printer used in this project; 0.8mm, and 1.2 mm. Moreover, we also tried to put the array into the locking bar and see whether it affects the performance of the mechanism.

We match the actuation force that we use to pinch force value from the literature force that is sufficient for daily activities , which is 30 N [51] with several assumptions of transmission ratio; 30 N resembling >90% transmission rate, 40 N resembling 75% transmission rate, 60 N resembling 50% transmission rate. All the specimens we use are shown in Table xvi and the result is shown in Figure 33 and Figure 34 (normalized for the pinch force drop percentage).

From Figure 33, we observed that the DG specimen could retain higher force in comparison to the other specimens. If we look at the normalized graph in Figure 34, double groove specimens can retain more than 90% of the force introduced to the locking mechanism. The performance from A 1.2 specimens performs similarly to the control specimens, while being worse in comparison to the A 0.8 specimens. Putting the groove in the locking bar seems to increase the value of the force retained better compared to the value from putting the groove in the locking surface, as shown by TG and A 0.8 specimen, while putting the groove in both locking bar and locking surface increases the force retained by the mechanism even more as shown by the DG specimen

Table xvi. Specimen's codename and CAD picture

Codename	Specimen	CAD	Codename	Specimen	CAD
C	Control specimen		A 1.2	An array of 1.2mm triangle	
A 0.8	Array of 0.8mm triangle		TG	An array of 0.8mm triangle in the locking bar	
DG	An array of 0.8mm triangle in both surface and locking bar				

Figure 33. Force retained by the spring across different specimen with different surface topology.

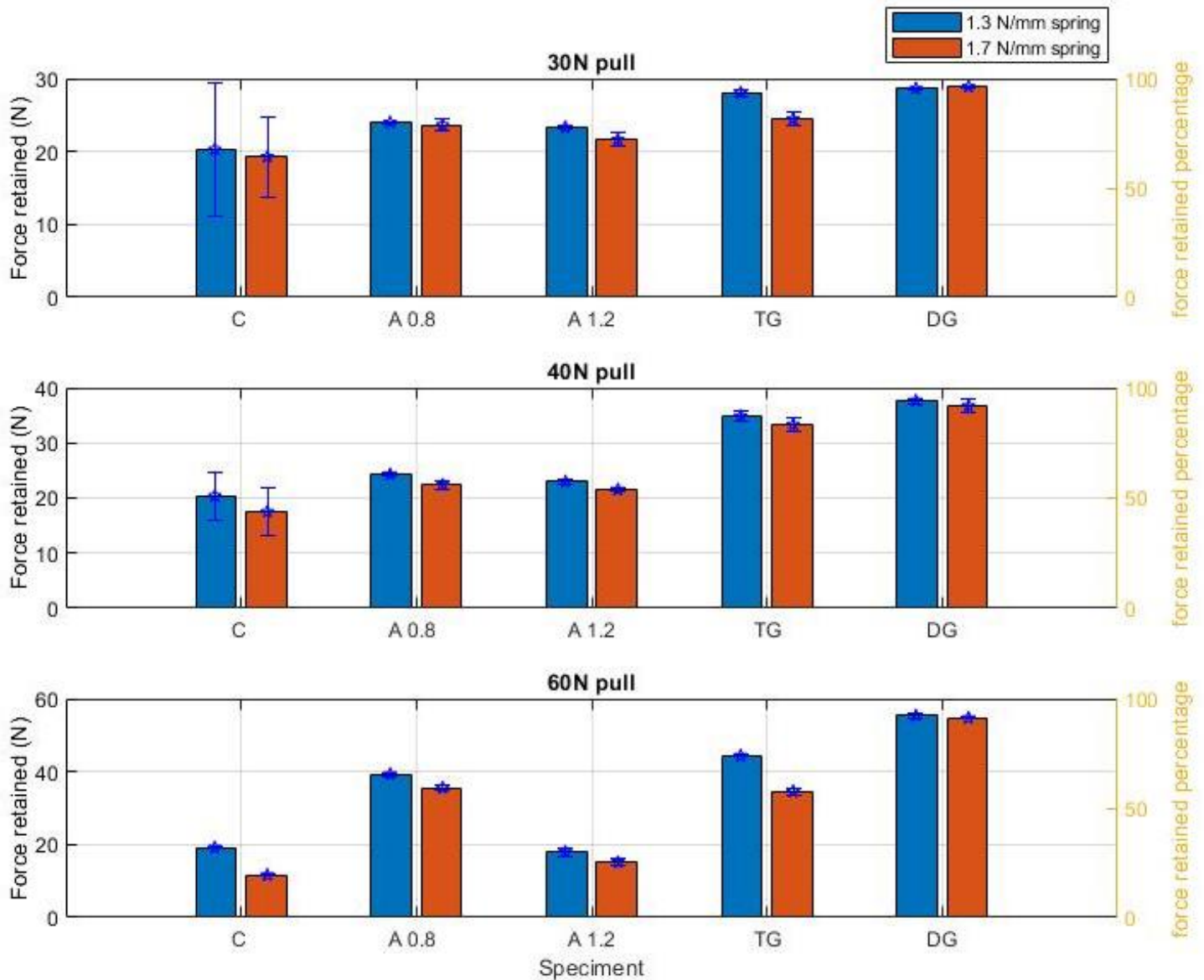


Figure 34. Geometry to increase surface friction, normalized for force retained percentage

5.2.4 The effect of different cable material

In this section, we will evaluate the effect of different cable material to the performance of the locking mechanism. The double groove specimen is used with the 1.7 N/mm spring using three other cables; a stronger nylon cable, fishing wire and steel. We present the specification of all cable we used in Table xvii . Wire sleeve is the amount of fiber strand use to wrap the core wire. Maximum weight, in this case, is presented in the wire product itself. We will assume the maximum weight is equivalent on the maximum loading this wire can take before yielding.

In the result, which we show in Figure 35, we can see that the performance difference from the fishing line wire and rest of the wires at 30 N pull and 40 N pull is less than 3N, while the performance difference from 60 N pull is almost 10 N. After the 60 N pull, fishing line wire undergone a visible plastic deformation, which we showed in Figure 36. Nylon 1, nylon 2, and poly propylene wire have a similar result of their performance at 60N pull. For the case of using steel wire, DG specimen could not achieve a locking because the steel cable scratches the locking bar part of the DG specimen, ultimately breaking the specimen.

Table xvii. Wire specification

	Nylon 1 (used previously)	Nylon 2 (stronger nylon)	Fishing line	Polypropylene	Stainless Steel
diameter (mm)	3	3	1.5	4	1.5
max weight (N)	294.3	1883.52	222.68	4000	Not disclosed
wire sleeve (amount of fiber)	16	16	no sleeve	20	7
wire core (amount of fiber)	3	3	1	3	no core
Static friction coefficient (N/m)	0.28	0.28	Not disclosed	0.37	0.27

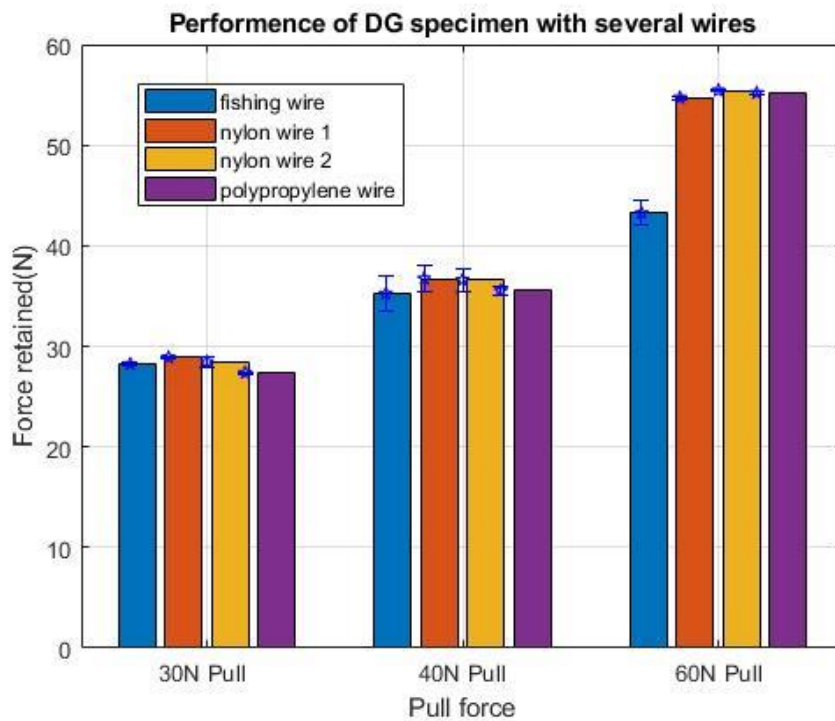


Figure 35. DG performance with nylon and fishing wire



Figure 36. Visible deformation in the fishing wire

Because the two nylon wires and the polypropylene wire exhibit similar performance, we redo this pull test using a spring of 2 N/mm coefficient with 120 N pull force. This number is used to imitate prosthesis with 25% transmission rate to achieve 30 N pinch force. Figure 37 shows the result of this measurement. We can see that while Nylon 2 wire have almost six times strength compared to Nylon 1 wire, Nylon 2 wire only have a slight performance increase.

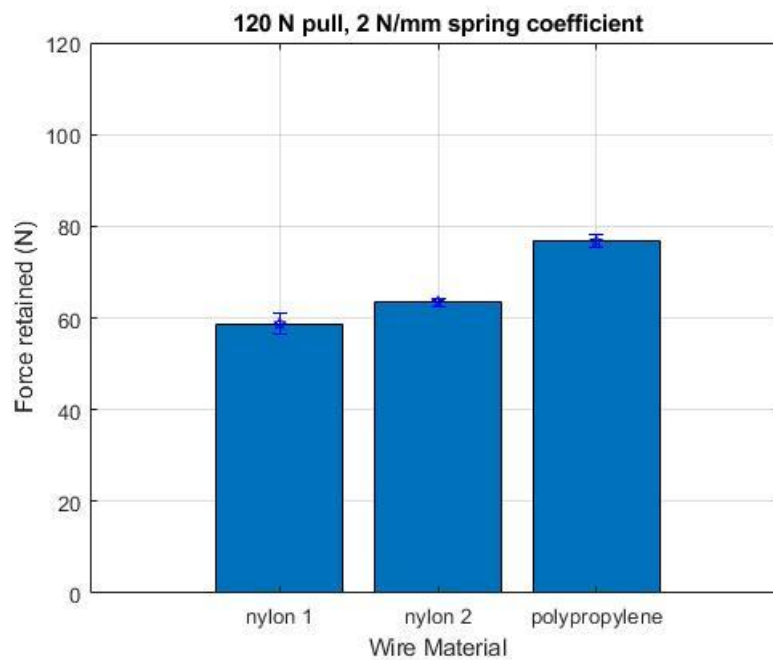


Figure 37. Maximum performance from DG specimen with respect to different wire material.

5.3 Discussion

As we can see from Figure 33, the shaft printed in the horizontal build specimens are printed with poorer precision relative to the vertical build specimens. This might happen because in the layer height used in this project is 0.3 mm, as we discussed prior in chapter 3.5.1, which affects how the perimeter of the shaft is formed. Per the self-energizing principle, we know that the alignment between the locking bar and the locking surface needs to be precise. While using a smaller layer height might improve the quality of the shaft, by just printing the shaft using the vertical build configuration, we can already print the shaft with higher quality circle. As we can see from the result of the vertical build specimens, their print accuracy makes the force drop value more consistent across all the samples.

By comparing the result from specimen A1.2 and A0.8, we could say that an array of triangle with smaller in size, generally, leads to a surface with higher coefficient of friction. Because we know that Petterson did the modification in a scale of around 50 microns, we hypothesize that this modification is fruitful up to around that value and we will get surfaces with higher coefficient of friction the smaller the triangle array gets. In the future, if the resolution of FDM 3D printing machine gets up to this level of precision, we will be able to test this hypothesis.

If we look at the performance from the DG specimen across Figure 33 and Figure 37, we know that the performance limit of this specimen is around 60N across 60N pull, and 120N pull for nylon 1 material. This trend is somewhat similar to the result we get from the control specimens and the A1.2 specimens in Figure 33 where they have a limit of the maximum force they can retain; which number does not go up should we increase the activation force. This phenomenon contradicts the calculation theory of a self-energizing brake because the locking moment scales indefinitely with the moment created from the hand force.

We hypothesize that the phenomenon happened because the value of hand force is not converted entirely into the normal force that goes to the calculation and some of the hand force contributes to the deformation of the cable. If we assume all transmission cable of a prosthesis system is made from a linearly elastic material, then the cable can only be subjected by force up until a limit is reached. The fact that fishing wire can only hold up to around 40 N of force, which is shown in Figure 36, until it is plastically deformed might be the evidence of this phenomenon.

Interestingly, Nylon 2 has only a little higher performance value compared to nylon 1 despite having almost six times the strength. We think this happen because the strength featured in the specification is the strength in the axis along' their length not the perpendicular to its length, which is the direction of the loading experienced by the cable. To fully investigate the effect of these wire, we need to perform more elaborate study with the specification of these wire as the variable, such as wire with same material and diameter but with different core and sleeve configuration.

At this moment, we know that polypropylene wire can hold most force in comparison to other material. We will assume that this happened simply because its coefficient of friction is the highest among all other wire, not due to its strength per aforementioned example of Nylon 1 and 2. Another point that indicate that wire strength plays minor role is that the strength of Nylon 1 is not far from the strength of fishing line wire, despite fishing line did undergo a visible plastic deformation at a lesser loading.

6

6. Prototype design

6.1 Frame

For the frame, to comply with our previously introduced design criteria in chapter 3.2, we will put the locking mechanism inside the forearm to minimize features with “sticking-out edges”. As a result, the forearm will still be like a natural looking forearm. The input dimensions used for this design is the hand width (HW) and hand thickness (HT), both of which are taken from DINED2004 Dutch adult database as can be seen in Figure 38 . HT value taken from item 48 (hand thickness) plus item 45 (thumb breadth). HW value is taken from item 44 (Hand width without thumb) minus item 46 (forefinger breadth). The minimal and maximal size that will be utilized from the database is shown in Table xviii. As can be seen in Figure 41, we attached the locking surface inside the frame (encircled in red). In the design, the frame will feature an inner layer that is shaped as a circle the HT value as its diameter. This inner layer is helpful to print the outer layer without support

Table xviii. Minimum and Maximum value of several parameters for the parametric design

	HT	HW
average	48 mm	68 mm
minimum*	30 mm	49 mm
maximum	56 mm	77 mm

*The minimum value is 10 mm less from the minimum value found in the database to compensate for people with smaller hand size.

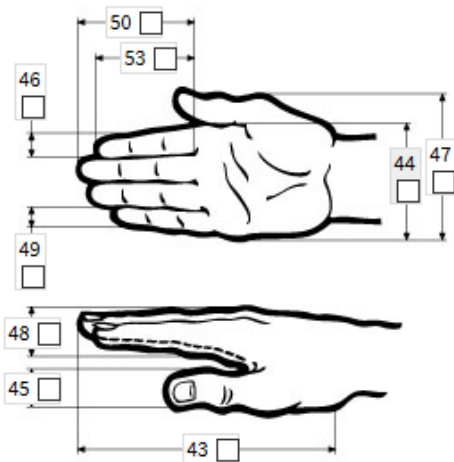


Figure 38. DINED2004 Dutch adult database

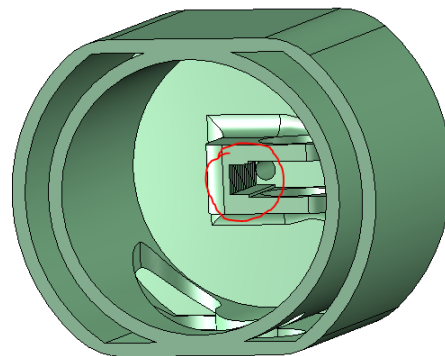


Figure 39. Initial frame design.

6.2 Handle

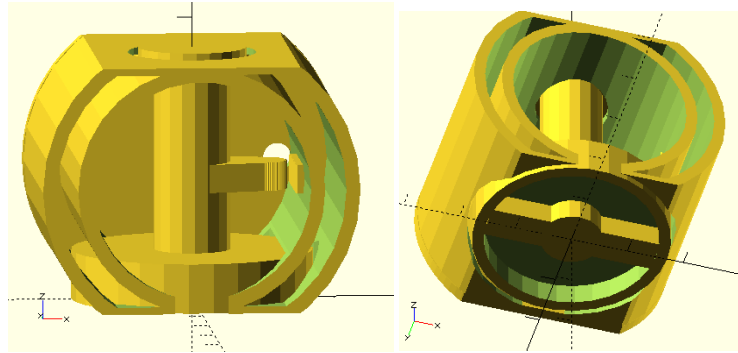


Figure 40. Handle design A

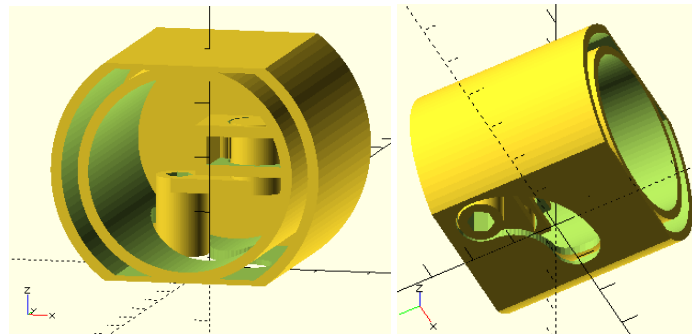


Figure 41. Handle design B

The handle will contain the locking bar printed with clearances corresponds to the configurations in Chapter 4. We consider 2 design of the handle (design A and design B), which we present in Figure 40 and Figure 41. In design A, the rotating shaft that connects to the locking bar touches the build plate of the bed of the 3D printer via the handle. This ensure easier printing. However, due to the height of the shaft, the locking bar are more prone to vibration. In design B, the rotating shaft is not printed directly from the build plate, thus making printing more difficult through the introduction of more supports. However, the shaft is less prone to vibration because the shaft is not as long. In the end we chose design B because the vibration might reduce the performance of the locking mechanism

We created a hexagonal hole and the rough surface on the end to help the patient to operate the locking mechanism by making it easier to grip. Additionally, the hexagonal hole helps the mechanism to turn, which might be harder directly after printing due to residual support. We present the full system of the locking mechanism in Figure 43. Section view of the locking mechanism Figure 43 and Figure 44

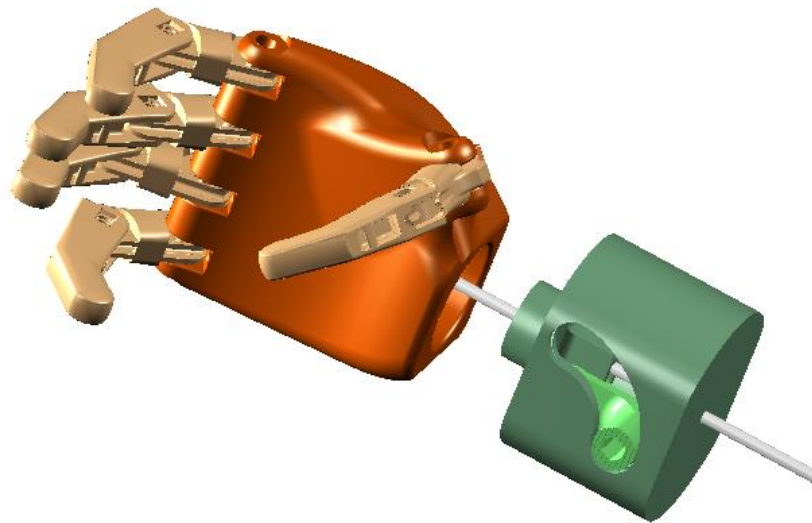


Figure 42. Full prosthesis system for right hand (orange = hand, teal = frame, green = handle, white = cable)

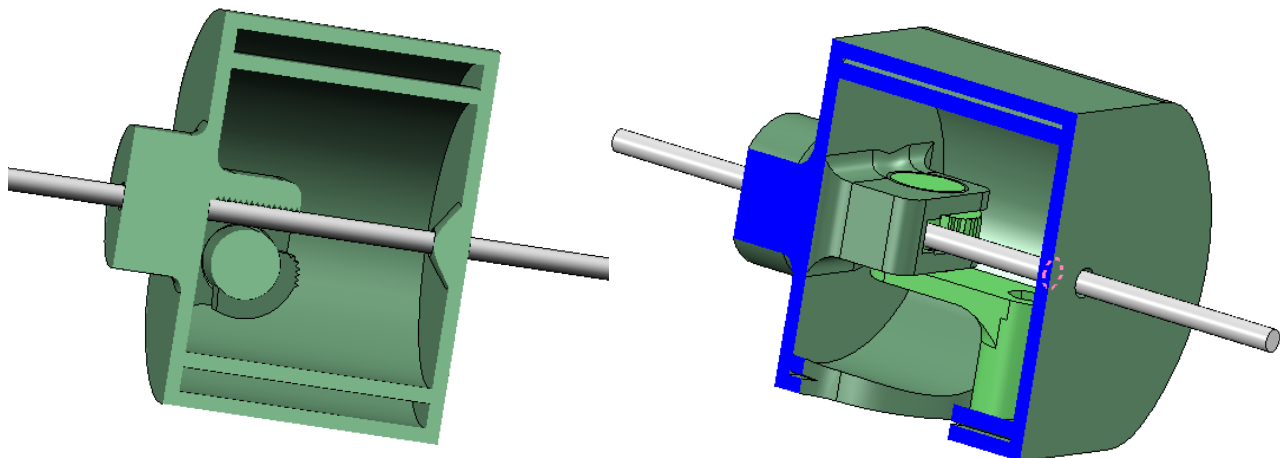


Figure 43. Section view of the locking mechanism

6.3 Parametric input

We use parametric design to accommodate the maximum and minimum dimension. Parametric design also helps to accommodate several variations of nozzle size which affects the clearance of parts. In this case, we utilize an open source, python-based software called Openscad. Figure 44 shows all the input parameter for this design and the contributing output of each parameter. In Figure 45, we can see the corresponding result of this parametric variation.

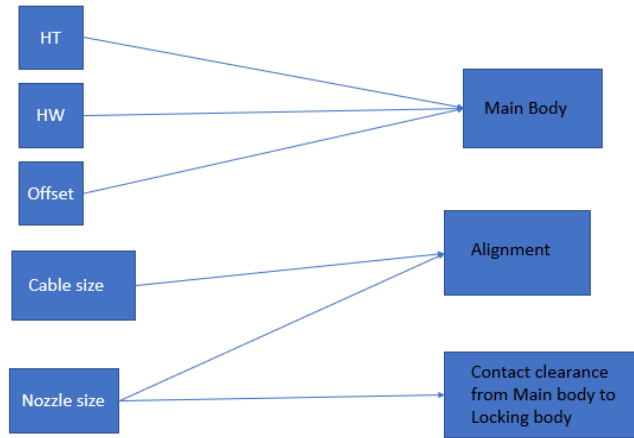


Figure 44. Input design parameter and their corresponding output

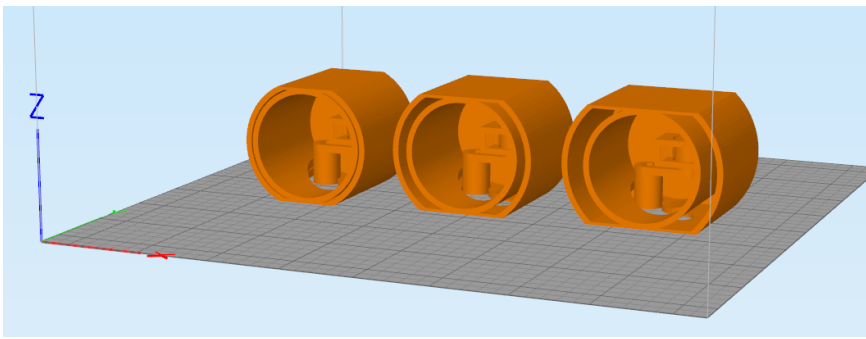
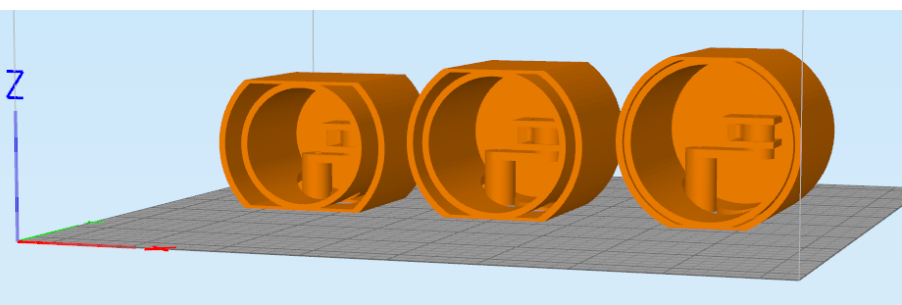
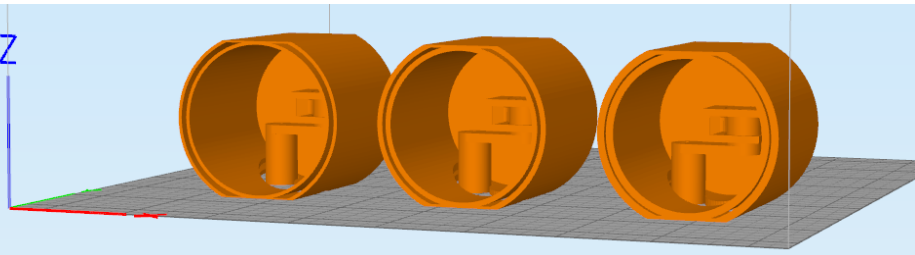
HW	Left to Right: 45 mm, 50 mm, 55 mm
HT = 40	
HT	Left to Right: 45 mm, 50 mm, 55 mm
HT = 55	
Offset	Left to Right: 1.0 mm, 1.5 mm, 2.0 mm
HTxHW = 45x50	

Figure 45. Example of different parameter input (HT, HW, and offset)

A printer with smaller nozzle size can result in part with higher accuracy. This accuracy affects the contact clearance between the main body (which contains the frame and the locking surface) and the locking body (which contains the locking bar and the handle). In the code, we put the clearance to be 0.1 mm higher from the nozzle size of the printer. Figure 46 shows effect of the nozzle size to the design

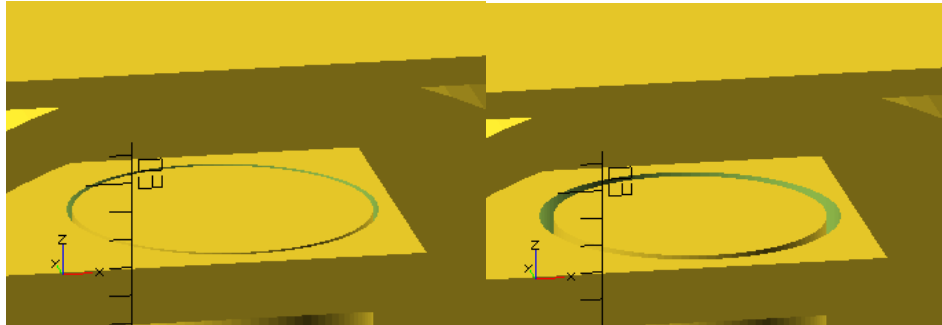


Figure 46. Effect of nozzle size to the clearance (left = 0.1 mm nozzle size, right = 0.4 mm nozzle size)

We will also allow a variation for the height of the cable relative to the bottom shell of the locking mechanism in the case of the transmission cable does not run precisely in the middle of the alignment, as can be seen in Figure 47. We present the realization of the part in Figure 48

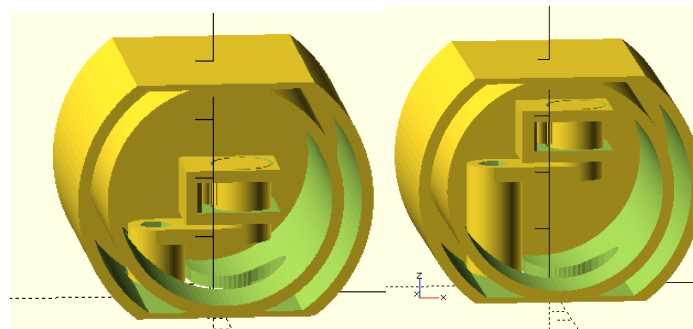


Figure 47. Height difference for the locking bar



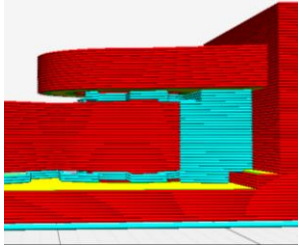
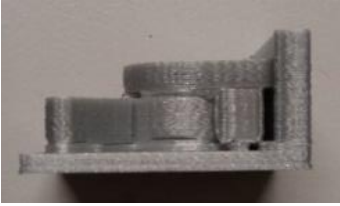
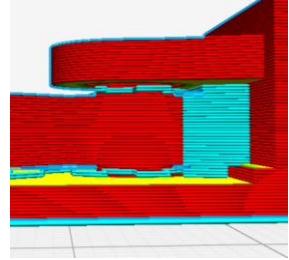
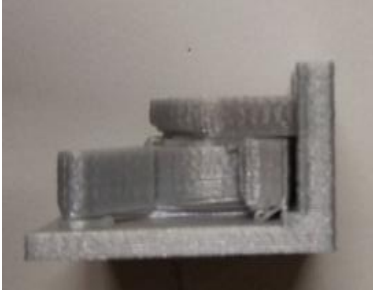
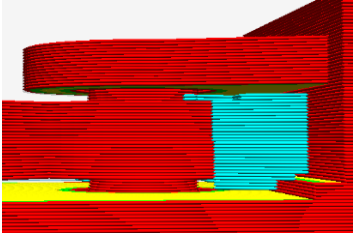
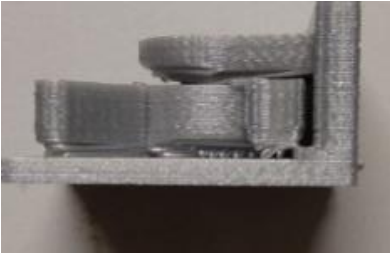
Figure 48. Realization of the full prototype

6.4 3D printing process

There are 3 possible z-support configurations in Cura; No support, gull support, and half support. In the Full support configuration, the overhanging structure will be in full contact from the support, while in the hanging support only the bottom surface is in contact with the support. In the no support configuration, there is no support involved. As can be seen in the realization column of Table xix, all 3 supports print without any functional problem. Based on the writer's experience in removing the support from these specimens, the no support configuration feels easier to remove while the full support configuration feels harder to support.

There are six default support design in Cura; lines, grid, triangle, concentric, zig-zag, and cross. Higher density can result in lower bridging distance for overhanging parts. For this project, we chose the triangle distance with 10% density because the support makes a closed structure thus make easier removal.

Table xix. Z-Support possible configuration in Cure (support is represented in blue lines)

Name	Cura Picture	Realization
<p>Full support</p>		
<p>Hanging support</p>		
<p>No support</p>		

7. Evaluation of the final prototype

7.1 Methodology

In this section, we will compare how the prototype fares in comparison to previous, commercially available locking mechanisms. Thus, we will use a full prosthesis system as opposed to a spring to simulate a prosthesis we do in chapter 5. In this case, we use DIPO lab's original test bench [11], which setup can be seen in Figure 49 and detail we provided in Table xx. The protocol of this testing follows Gerwin's [11] and Gemmell's [10] protocols from their respective publications. The sequences are: (1) set the pinch force to acquire 15 N (Gerwin) /45N (Gemmell), (2) lock the mechanism, (3) release the activation force, (4) reapply the activation force and release locking the mechanism. The hand used in this experiment is TRS hook. We will test 2 sample with one using Nylon 2 wire and the other using Polypropylene wire both of which featured in chapter 5.2.4.

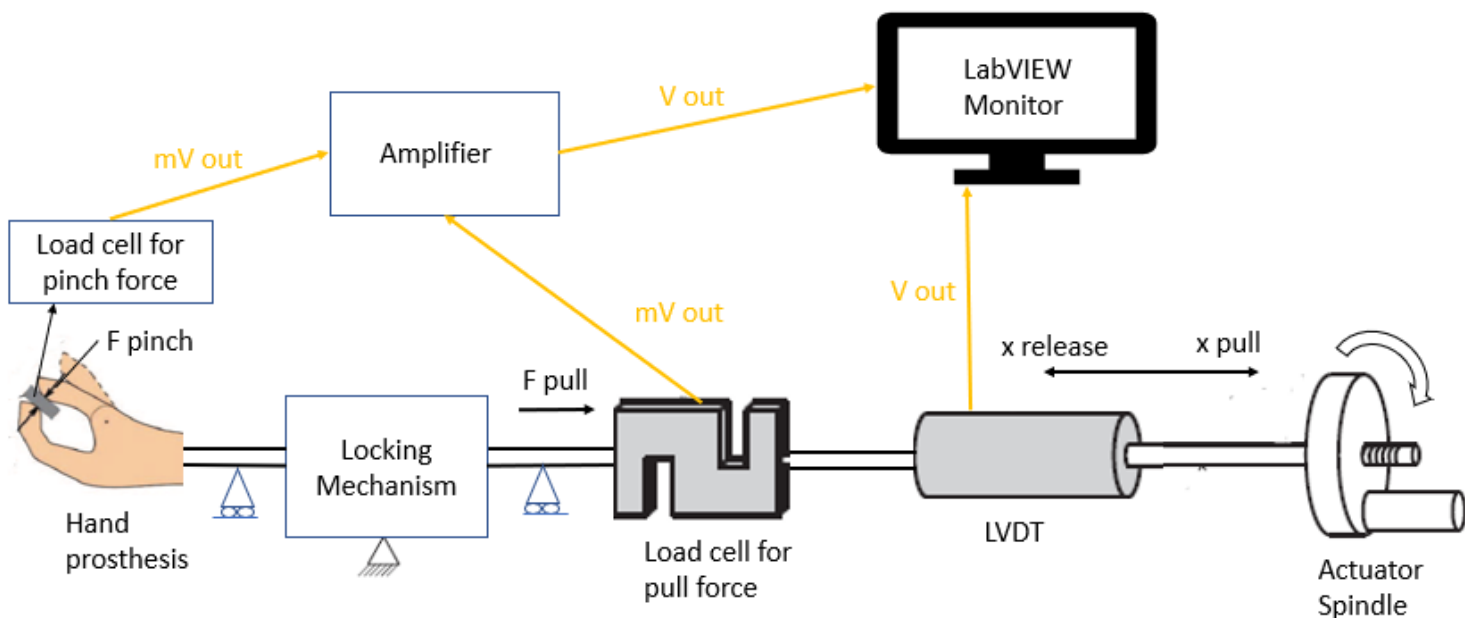


Figure 49. Test bench used for the final evaluation

Table xx. Spesification for the 2nd test bench

Components	Spesification
Load cell (activation force)	Zemic: FLB3G-C3-50kg-6B
Amplifier	Scaime: CPJ
LVDT	Schaevitz: LCIT 2000
Load cell (pinch force)	Double leave spring with strain gauges
USB interface	National Instruments: NI USB-6008

7.2 Result

7.2.1 15N pinch force

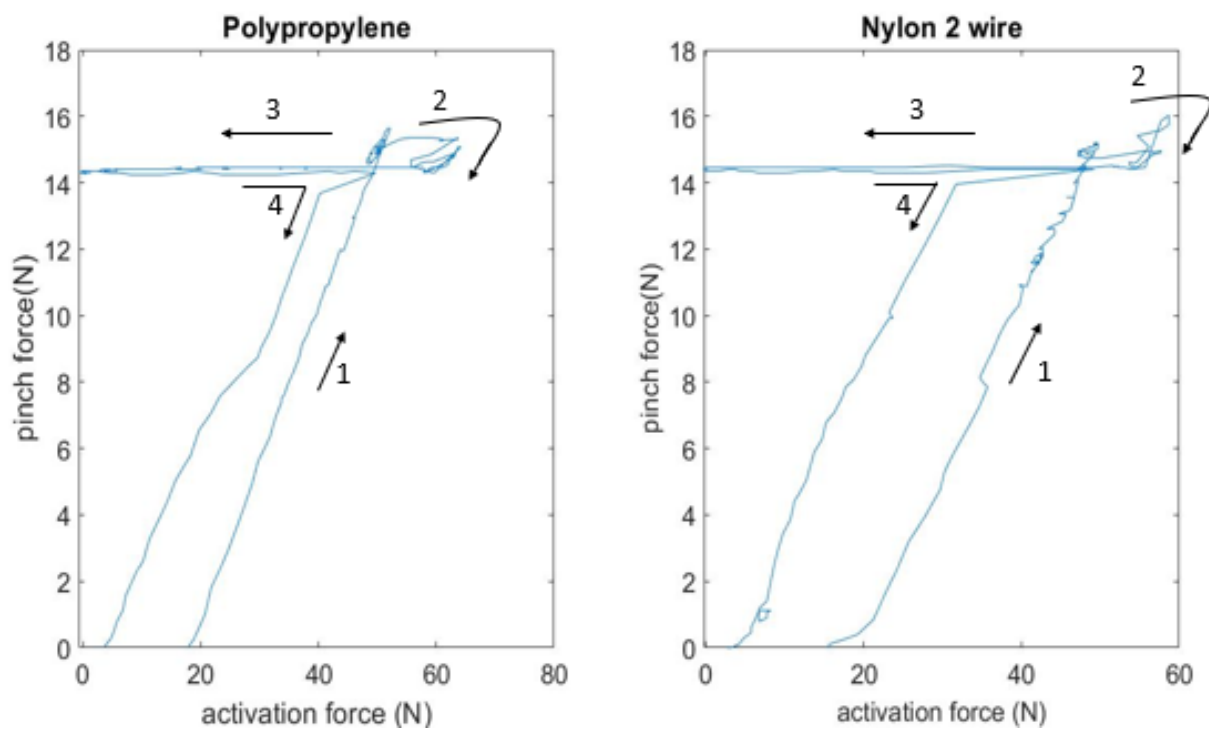


Figure 50. Activation force vs pinch force diagram of sample printed using polypropylene wire and nylon 2 wire. (1) set the activation force to acquire 15 N pinch force (2) engage the lock (3) release the activation force, (4) reapply the activation force and release locking the mechanism

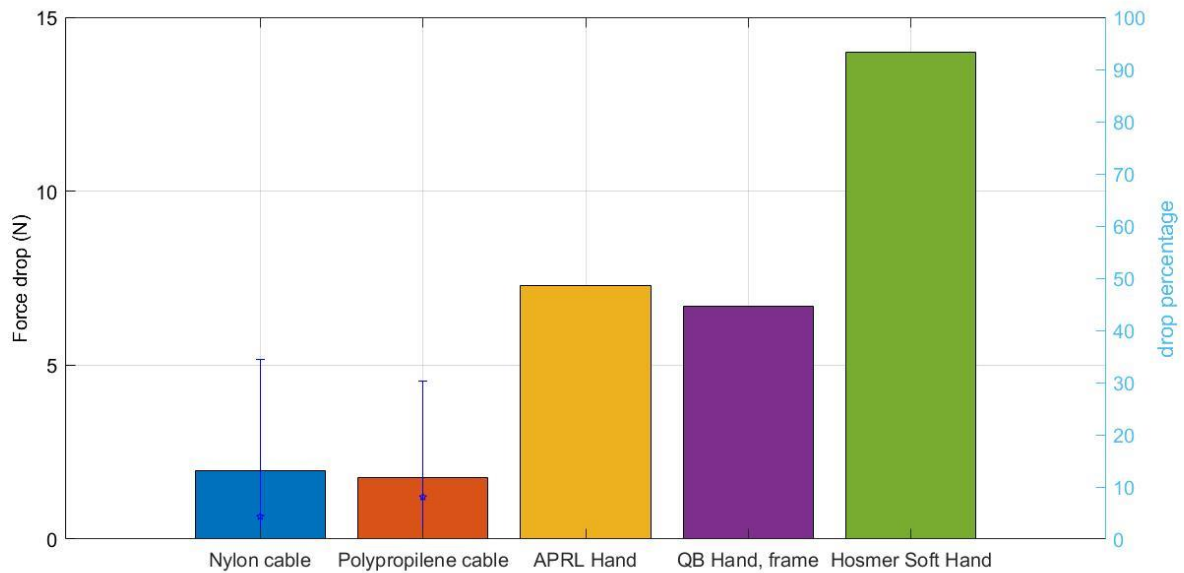
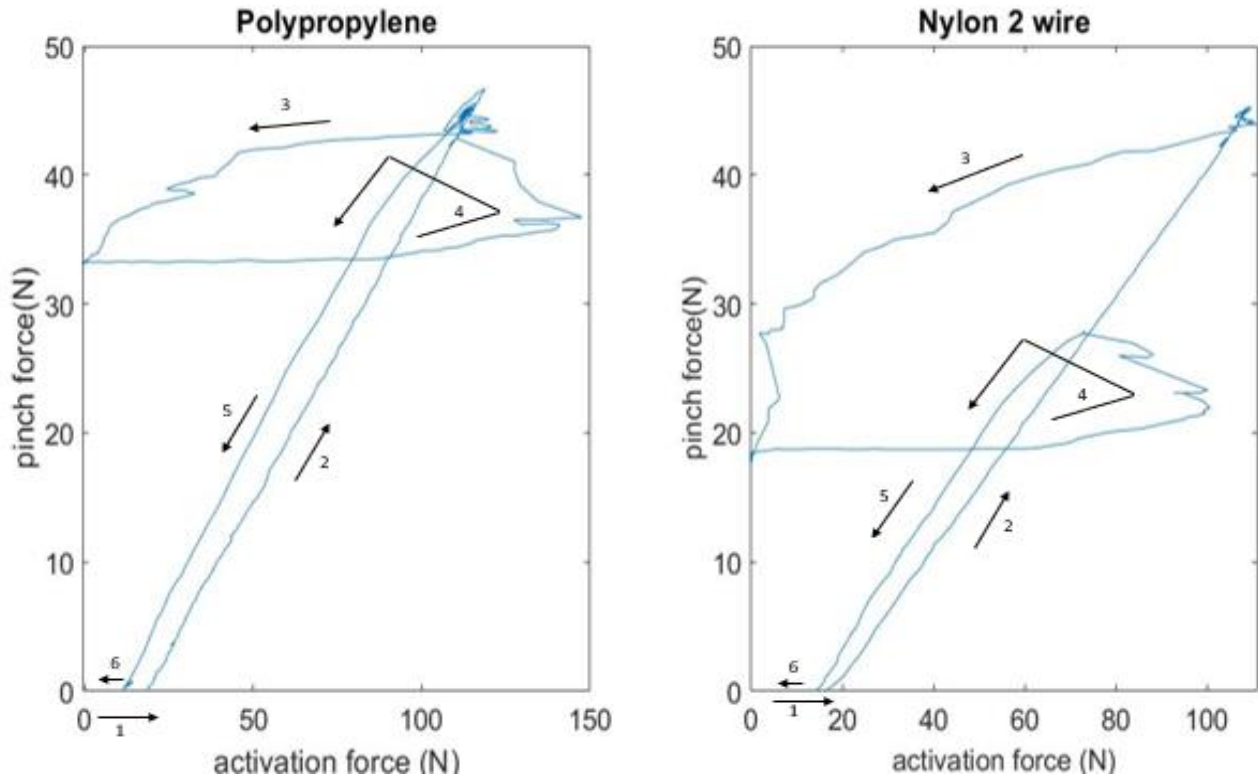


Figure 51. Performance of this locking mechanism in comparison with several commercially available locking mechanism (source : [11], minus the error bar.)

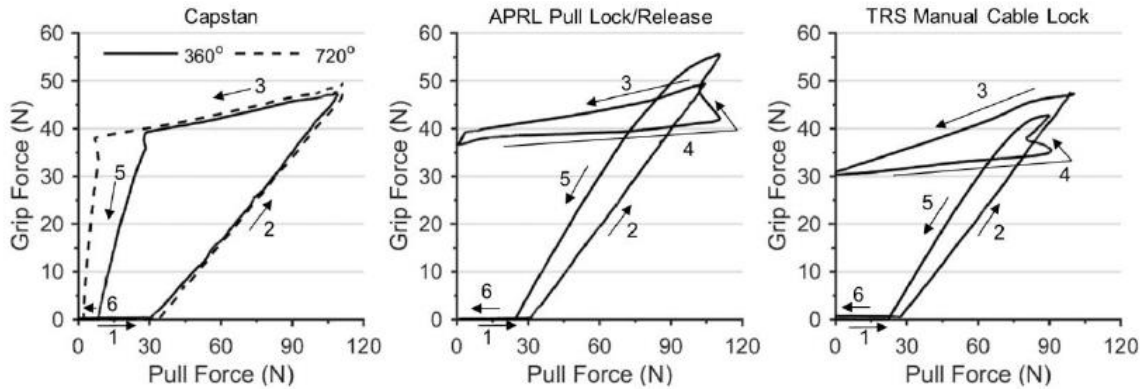
As can be seen from Figure 50, the 4 arrows represent each sequence of the test from the protocol. We can see that the samples, both of which uses slightly different input parameter respectively for the diameter of Nylon 2 and polypropylene wire, produces similar output graph. The pinch force start rising after around 20N of activation force is given through the spindle and reaches around 45 N to achieve 15 N pinch force. This indicates that the transmission ratio of this prosthesis is around 0.6 between pinch force and activation force. Next, the process of engaging the lock in this mechanism increases the force detected by the activation force sensor by +20 N. After we engaged the lock, both samples exhibit a minimal pinch force drop value, retaining more than 14 N pinch force.

From 3 instances of experiment, we get the average of pinch force drop for the specimen using Nylon 2 wire is 1.95 N while the pinch force drop for the specimen using Polypropylene wire is 1.77 N. We provide a comparison of this value to the pinch force drop value of several other prosthesis with locking mechanism in Figure 51 If we compare the performance from these samples to the sample in the literature, we can see that this locking mechanism has the least amount of force drop.

7.2.2 45N pinch force



(a)



(b)

Figure 52. Result of 45N pinch force test. (a) for this 3D printed locking mechanism, (b) the result of Gemmell's experiment [10]. (1) Start giving activation force (2) finger close and start to give pinch force as we further increase the activation force (3) locking is engaged, removal of the activation force (4) reapply the activation force to release locking the mechanism (not applicable to the capstan lock). (5) Decreasing the activation force. (6) finger open

For the 45 N comparison, we will use the data of three different prosthesis setup Gemmell provide in his study; TRS Manual Cable lock, APRL Pull Lock/ Release, and Capstan based locking mechanism he created on his own for his study. In this scenario, we can see that the locking mechanism perform worse compared to when its holding 15N of pinch force. More specifically, the sample using polypropylene can hold around 33N pinch force

while the sample using nylon 2 wire can only hold 20N pinch force. Comparing our result with the result from Gemmell's publication, this locking mechanism using polypropylene wire can comparably hold pinch force as much as TRS's Manual cable lock while Gemmell's locking mechanism and APRL pull still performed better. Using Nylon 2 wire resulting in the hugest amount of pinch force drop.

7.3 Discussion

The result for we get in this chapter is consistent with the result we get in chapter 5.2.4. In the case of 15N pull, per Figure 50, the activation force required to reach 15N of pinch force doesn't exceed 60N. If we look back to Figure 34, we know that DG specimen with nylon and polypropylene can hold 60 N spring force with minimal force drop. This similarity also happened in the case of 45N pull. If we compare the result we get from Figure 51 and Figure 37. In both figures, the locking mechanism with polypropylene wire can hold higher pinch force in comparison to the locking mechanism with nylon wire. Because final prototype of this locking mechanism performs similarly to the samples we use in chapter 5, we can assume that any kind of shape for a PLA 3D printed locking mechanism using self-energizing principle will have similar performance as long as the 2 surfaces that comes in contact with the wire is shaped similarly to the DG specimen. Should we use a prosthesis that have higher transmission ratio, we should be able to hold pinch force in a higher value.

Conveniently, 3 prosthesis that Gemmell utilized in his study each follow one of the six conceptual solution we introduced in chapter 3; TRS hand uses shape lock directly to the cable, APRL pull uses shape lock through an interface (which is a ratchet mechanism to keep the hand closed), and Gemmell's original solution uses shape lock through a winch. Comparing the result of this project with TRS hand, both of which uses self-energizing concept, the surface modification gives this 3D printed locking mechanism gives comparable result to the steel cable and steel locking surface that TRS uses. Interestingly, all three conceptual solution still leads to pinch force drop.

In conclusion, this locking mechanism have several advantages compared to other locking mechanism;

1. In a low pinch force region, this locking mechanism will yield in less pinch force drop compared to several other prosthesis hand system
2. In a high pinch force region, this locking mechanism performs comparably in comparison to several other prosthesis hand with different conceptual solution.
3. This locking mechanism is fully 3D printed in one go by using non-assembly mechanism and compliant with user's hand dimension by using parametric design. That means this locking mechanism is personalized and can be used straight after the 3D printing process.

8

8. Conclusion and future works

8.1 Conclusion

We designed a 3D printed locking mechanism for transradial hand prosthesis using PLA via FDM 3D printing. The locking mechanism is based on a self-energizing brake with modified surface topology at the two contact surfaces between the PLA and the cable. The design satisfies these design criteria as follows; (1) can be pulled with more than 600 N force, (2) weight as low as less than 50 grams included within the forearm, (3) follows the shape of a natural forearm and feature no sharp edges, and (4) can be fabricated with no assembly required. We use parametric design so that the locking mechanism can compensate for various sizes of patient's arm, various printers, and various cable material.

We fabricated the locking mechanism in 1 assembly direct after printing using a non-assembly mechanism by which we use clearance value of the locking bar part and the frame that varies according to the nozzle diameter of the 3d printer. Non-assembly mechanism lessens the work required after printing so that patient can directly use the locking mechanism without any consultation to medical personnel that might be rare in developing countries.

We evaluated the locking mechanism by measuring the magnitude of the force it can retain after we engaged the lock. Using polypropylene wire, this mechanism can hold up to around 75 N force from the hand. Using TRS Hook, the locking mechanism experienced less than 1 N force drop if we use the hook to give 15 N pinching force and around 12 N force drop if we give 45 N pinching force. This value varies with the wire material utilized

8.2 Future works

In the future, the performance of this locking mechanism can be improved by doing extensive research about the wire utilized in conjunction with the mechanism. Moreover, with the advancement of 3D printing machine, a better locking surface can be investigated by fabricating a smaller triangle array. Lastly further study regarding the wear of this locking mechanism, especially on the locking surface, can be done using fatigue testing to validate the lifespan of this mechanism which we calculate back in chapter 4 that results in the utilization of the self-energizing concept in the first place.

Appendix

References

1. Staats, T. B. The rehabilitation of the amputee in the developing world: a review of the literature. *Prosthet. Orthot. Int.* **20**, 45–50 (1996).
2. Pooja, G. Das & Sangeeta, L. Prevalence and aetiology of amputation in Kolkata, India: A retrospective analysis. *Hong Kong Physiother. J.* **31**, 36–40 (2013).
3. Thanni, L. O. A. & Tade, A. O. Extremity amputation in Nigeria - A review of indications and mortality. *Surgeon* **5**, 213–217 (2007).
4. Kim, Y. C., Park, C. I., Kim, D. Y., Kim, T. S. & Shin, J. C. Statistical analysis of amputations and trends in Korea. *Prosthet. Orthot. Int.* **20**, 88–95 (1996).
5. Sarvestani, A. S. & Azam, A. T. Amputation: A ten-year survey. *Trauma Mon.* **18**, 126–129 (2013).
6. Carey, S. L., Lura, D. J., Highsmith, M. J., CP & FAAOP. Differences in myoelectric and body-powered upper-limb prostheses: Systematic literature review. *J. Rehabil. Res. Dev.* **52**, 247–262 (2015).
7. Zuniga, J. *et al.* Cyborg beast: a low-cost 3d-printed prosthetic hand for children with upper-limb differences. *BMC Res. Notes* **8**, 10 (2015).
8. Xu, G. *et al.* Three-dimensional-printed upper limb prosthesis for a child with traumatic amputation of right wrist. *Med. (United States)* **96**, e9426 (2017).
9. Hichert, M., Vardy, A. N. & Plettenburg, D. Fatigue-free operation of most body-powered prostheses not feasible for majority of users with trans-radial deficiency. *Prosthet. Orthot. Int.* **42**, 84–92 (2018).
10. Gemmell, K. D., Leddy, M. T., Belter, J. T. & Dollar, A. M. Investigation of a passive capstan based grasp enhancement feature in a voluntary-closing prosthetic terminal device. *Proc. Annu. Int. Conf. IEEE Eng. Med. Biol. Soc. EMBS 2016–Octob*, 5019–5025 (2016).
11. Smit, G. & Plettenburg, D. H. Efficiency of voluntary closing hand and hook prostheses. *Prosthet. Orthot. Int.* **34**, 411–427 (2010).
12. Borg, J., Lindström, A. & Larsson, S. Assistive technology in developing countries: national and international responsibilities to implement the Convention on the Rights of Persons with Disabilities. *Lancet* **374**, 1863–1865 (2009).
13. Magnusson, L. & Ahlström, G. Experiences of providing prosthetic and orthotic services in Sierra Leone - The local staff's perspective. *Disabil. Rehabil.* **34**, 2111–2118 (2012).
14. Marino, M. *et al.* Access to prosthetic devices in developing countries: Pathways and challenges. *Proc. 5th IEEE Glob. Humanit. Technol. Conf. GHTC 2015* 45–51 (2015). doi:10.1109/GHTC.2015.7343953
15. Ibrahim, A. M. S. *et al.* Three-dimensional Printing in Developing Countries. *Plast. Reconstr. Surg. - Glob. Open* **3**, e443 (2015).
16. Baden, T. *et al.* Open Labware: 3-D Printing Your Own Lab Equipment. *PLoS Biol.* **13**, 1–12 (2015).
17. Gibson, I., Rosen, D. & Stucker, B. *Additive Manufacturing Technologies. Rapid Manufacturing Association* (2013). doi:10.1520/F2792-12A.2

18. Chantarapanich, N., Puttawibul, P., Sitthiseripratip, K., Sucharitpwatskul, S. & Chantaweroad, S. Study of the mechanical properties of photo-cured epoxy resin fabricated by stereolithography process. *Songklanakarin J. Sci. Technol.* **35**, 91–98 (2013).
19. Dulieu-Barton, J. M. & Fulton, M. C. Mechanical properties of a typical stereolithography resin. *Strain* **36**, 81–87 (2000).
20. Hague, R., Mansour, S., Saleh, N. & Harris, R. Materials analysis of stereolithography resins for use in Rapid Manufacturing. *J. Mater. Sci.* **39**, 2457–2464 (2004).
21. Dizon, J. R. C., Espera, A. H., Chen, Q. & Advincula, R. C. Mechanical characterization of 3D-printed polymers. *Addit. Manuf.* **20**, 44–67 (2018).
22. Salmoria, G. V., Hotza, D., Klauss, P., Kanis, L. A. & Roesler, C. R. M. Manufacturing of Porous Polycaprolactone Prepared with Different Particle Sizes and Infrared Laser Sintering Conditions: Microstructure and Mechanical Properties. *Adv. Mech. Eng.* **2014**, (2014).
23. Song, Y. *et al.* Measurements of the mechanical response of unidirectional 3D-printed PLA. *Mater. Des.* **123**, 154–164 (2017).
24. Ahn, S., Montero, M., Odell, D., Roundy, S. & Wright, P. K. Anisotropic material properties of fused deposition modeling ABS. *Rapid Prototyp. J.* **8**, 248–257 (2002).
25. Simplify 3D(r). Filament Properties Table. Available at: <https://www.simplify3d.com/support/materials-guide/properties-table/>. (Accessed: 18th May 2018)
26. Ziemian, C. W., Ziemian, R. D. & Haile, K. V. Characterization of stiffness degradation caused by fatigue damage of additive manufactured parts. *Mater. Des.* **109**, 209–218 (2016).
27. Ziemian, S., Okwara, M. & Ziemian, C. W. Tensile and fatigue behavior of layered acrylonitrile butadiene styrene. *Rapid Prototyp. J.* **21**, 270–278 (2015).
28. Cuellar, J. S., Smit, G., Plettenburg, D. & Zadpoor, A. Additive manufacturing of non-assembly mechanisms. *Addit. Manuf.* **21**, 150–158 (2018).
29. Calignano, F. *et al.* Direct fabrication of joints based on direct metal laser sintering in aluminum and titanium alloys. *Procedia CIRP* **21**, 129–132 (2014).
30. Howell, L. L., Magleby, S. P. & Olsen, B. M. *Handbook of Compliant Mechanisms. II*,
31. Plettenburg, D. H. Basic requirements for upper extremity prostheses: the WILMER\approach. *Proc. 20th Annu. Int. Conf. IEEE Eng. Med. Biol. Soc. Vol.20 Biomed. Eng. Towar. Year 2000 Beyond (Cat. No.98CH36286)* **5**, 2276–2281 (1998).
32. Sensinger, J. W., Lipsey, J., Thomas, A. & Turner, K. Design and evaluation of voluntary opening and voluntary closing prosthetic terminal device. *J. Rehabil. Res. Dev.* **52**, 63–75 (2015).
33. Hichert, M., Abbink, D. A., Kyberd, P. J. & Plettenburg, D. H. High cable forces deteriorate pinch force control in voluntary-closing body-powered prostheses. *PLoS One* **12**, 1–13 (2017).
34. Smit, G., Plettenburg, D. H. & Van Der Helm, F. C. T. The lightweight Delft Cylinder hand: First multi-articulating hand that meets the basic user requirements. *IEEE Trans. Neural Syst. Rehabil. Eng.* **23**, 431–440 (2015).
35. Luchetti, M., Cutti, A. G., Verni, G., Sacchetti, R. & Rossi, N. Impact of Michelangelo prosthetic hand:

- Findings from a crossover longitudinal study. *J. Rehabil. Res. Dev.* **52**, 605–618 (2015).
36. FDM filament cost comparison. Available at: <https://www.3ders.org/pricecompare/>. (Accessed: 22nd May 2018)
 37. WANHAO STANDARD RESIN LIST REV . A Technical Data. 308058 (2017).
 38. Powders for SLS. Available at: <https://www.imakr.com/en/217-powders-for-sls>. (Accessed: 22nd May 2018)
 39. Jerez-Mesa, R., Travieso-Rodriguez, J. A., Llumà-Fuentes, J., Gomez-Gras, G. & Puig, D. Fatigue lifespan study of PLA parts obtained by additive manufacturing. *Procedia Manuf.* **13**, 872–879 (2017).
 40. Lee, J. & Huang, A. Fatigue analysis of FDM materials. *Rapid Prototyp. J.* **19**, 291–299 (2013).
 41. Charlton, I. W. & Johnson, G. R. A model for the prediction of the forces at the glenohumeral joint. *Proc. Inst. Mech. Eng. Part H J. Eng. Med.* **220**, 801–812 (2006).
 42. Mavroidis, C., DeLaurentis, K. J., Won, J. & Alam, M. Fabrication of Non-Assembly Mechanisms and Robotic Systems Using Rapid Prototyping. *J. Mech. Des.* **123**, 516 (2001).
 43. Carlson, LE, Frey, DD, Brown, E. Locking mechanism for voluntary closing prosthetic prehensor. (1976).
 44. John H. Loveless. Prosthetic load-lift hook locking mechanism.
 45. Veatch, B. D. Cable lock device for prosthetic and orthotic devices. (2005).
 46. Běhálek, L., Lenfeld, P. & Seidl, M. Friction Properties of Composites With Natural Fibres, Synthetic and Biodegradable Polymer Matrix. *Nanocon.Eu* (2012).
 47. Brown, W. E. *Friction Coefficients of Synthetic Ropes*. (NAVAL UNDERSEA CENTER SAN DIEGO CA, 1977).
 48. Khurmi, G. Textbook of Machine Design. in (SCH, 2017).
 49. Lalish, E. Gear Bearing. Available at: <https://www.thingiverse.com/thing:53451>. (Accessed: 19th May 2018)
 50. Pettersson, U. *Surfaces Designed for High and Low Friction*. Uppsala Universitet (2005).
 51. Keller, A. D. *Studies to determine the functional requirements for hand and arm prosthesis*. (Department of Engineering University of California, 1947).

3D printing process parameter

Cura version 3.3.1. Available at <https://ultimaker.com/en/products/ultimaker-cura-software>

Ultimaker 3 ▼

Extruder **1** | Extruder **2**

Material: PLA ▼

Print core: AA 0.4 ▼

[Check compatibility](#)

Print Setup | Recommended | **Custom**

Profile: Fine - 0.1mm ★ ▼

☰

Quality ▼

Layer Height	🔗 ↺	0.3	mm
Initial Layer Height	🔗 ↺	0.3	mm
Line Width		0.35	mm
Wall Line Width		0.35	mm
Outer Wall Line Width		0.35	mm
Inner Wall(s) Line Width		0.3	mm

Modified parameter :

- Layer height: 0.3 mm
- Initial layer height : 0.3 mm
- Infill density : 75%
- Infill pattern : Tri-Hexagon
- Print speed 40 mm/s
- Support placement : everywhere
- Support overhang angle : 85°
- Support pattern : ZigZag
- Support density : 10%
- Support Z distance : 3mm

Python code for the design

```
// Parametric process of a 3D printed locking mechanism for transradial hand prosthesis suitable for developing countries //
```

```
// Andika Praditya Hadiputra//
```

```
// Designed to acquire master degree at TU Delft biomedical engineering //
```

```
// supervised by Dick H. Plettenburg , Gerwin Smit, and Juan Cuellar Lopez Biomedical Engineering TU Delft //
```

```
////////////////////////////////////
```

```
////////////////////////////////input////////////////////////////////
```

```
////////////////////////////////////
```

```
a= 40; //Hand Thickness
```

```
b= 50; //Hand Width
```

```
ofset=2; // Wall thickness
```

```
cablesize=1.5; //cable size
```

```
nozzlesize=0.8; // printer's nozzle size
```

```
zz=0; // z distance from the hole (0 = precisely in the middle)
```

```
////////////////////////////////////
```

```
////////////////////////////////float////////////////////////////////
```

```
////////////////////////////////////
```

```
ppp=[[0,0.4],[0,-0.4],[-0.6268299345324,0]];
```

```
////////////////////////////////////
```

```
////////render////////////////////////////////
```

```
////////////////////////////////////
```

```

frame ();

cover();

translate ([-(3.6+cablesize/2),a/2-(12.68),zz+a/2-(offset + 2.5)])
lockingsuf ();

translate ([-(3.6+cablesize/2),a/2-(12.68),zz+a/2-(offset + 2.5)])
lockingbar ();

handle ();

////////////////////////////////////
////////////////////////////////////modules////////////////////////////////////
////////////////////////////////////

module frame (){

difference () // hole for handle operation
{
union() //union of inner shell and outer shell

{
translate([0,0,a/2])
rotate([90,0,0])
difference(){
cylinder(h=a, r1=a/2, r2=a/2, center=true,$fn = 100);
cylinder (h=a, r1=(a/2)-offset,r2=(a/2)-offset,

```

```

center=true,$fn = 100);}

difference(){
intersection(){
translate ([0,0,a/2])
rotate([90,0,0])
cylinder(h=a, r1=b/2, r2=b/2,center=true,$fn = 100);
translate ([0,0,a/2])
cube(size=[b,a,a],center=true,$fn = 100);}

intersection(){
translate ([0,0,a/2])
rotate([90,0,0])
cylinder(h=a+1, r1=(b/2)-offset, r2=(b/2)-offset,center=true,$fn = 100);

translate ([0,0,a/2])
cube(size=[b-offset,50,a-offset],center=true);}
}}
translate ([10.08-(2.62683+cablesized/2),a/2-(12.68/2),0])
{
for (i=[0:5:90])
rotate([0,0,i])
translate ([-3*a/8],0,0)
cylinder (h = a/2, r = 5.35, $fn = 30);

}
}

```

```

}
module cover (){
difference (){
intersection(){
translate ([0,(a/2)+(ofset/2),a/2])
rotate([90,0,0])
cylinder(ofset, r1=(b/2), r2=(b/2),center=true,$fn = 100);

translate ([0,(a/2)+(ofset/2),a/2])
cube(size=[b,50,a],center=true);}

translate ([0,0,a/2+zz])
rotate ([90,0,0])
cylinder (h = 100,r =cablesize+0.5,center = true, $fn = 30);
}
}

```

```

module lockingsuf () {

//shell
difference(){
difference(){

cube(size=[16,12.68,9.2]);

translate([2,0,2])
cube(size=[17,12.68,5.2]);}

translate ([10.08,6.34,0])

```

```

cylinder (h = 9.2,r1 = 5.35, r2 = 5.35,$fn = 100);}

//

rotate([0,0,180])
for (i=[0:0.4:12])
translate([-2,i-12.2,4.6])
linear_extrude(height = 5.2, center = true, convexity = 10, twist = 0)
polygon(ppp);
}

module lockingbar (){

//shaft
translate ([10.08,6.34,0])
cylinder (h = 9.2,r1 = 4.85, r2 = 4.85,$fn = 100);

//locking bar

translate([5.41,6.34,2.6])
for (i=[-102:12:102])
rotate([0,0,i])

union(){
translate([-1.65,0,0])
linear_extrude(height = 4, convexity = 10, twist = 0)
polygon(ppp);
translate([-1.65,-0.4,0])
cube(size=[1.65,0.8,4]);
}

```

```

// cable
//translate([2.6268,0,4])
//cube(size=[1.5,50,1.5]);

difference (){
union (){
{translate ([10.08,6.34,-3.6])
cylinder (h = 3.6,r1 = 4.85, r2 = 4.85,$fn = 100);

px = [[10.08,6.34+4.85],[10.08,6.34-4.85],[10.08-(3*a/8),6.34-4.85],[10.8-(3*a/8),6.34+4.85]];
translate ([0,0,-3.6])
linear_extrude(height = 2.6, convexity = 10, twist = 0)
polygon(px);}}

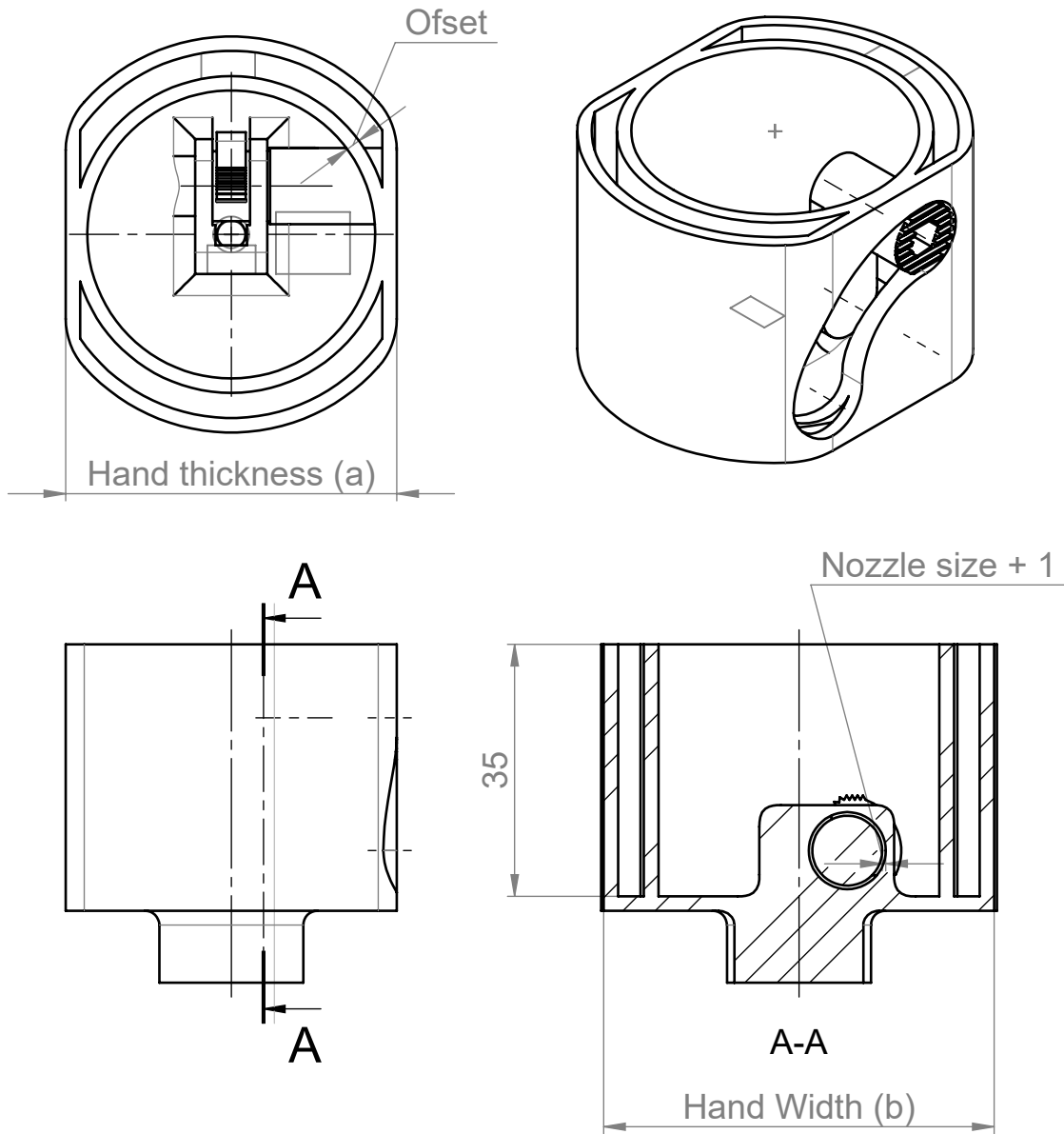
translate ([10.08-(3*a/8),6.34,-a/2])
cylinder (h = 20,r =3, $fn = 6);}

}

module handle (){
difference (){
translate ([10.08-(3*a/8)-(2.62683+cablesized/2),a/2-(12.68/2),0])
cylinder (h = zz+a/2-(ofset+2.5+1),r1 = 4.85, r2 = 4.85,$fn = 100);
translate ([10.08-(3*a/8)-(2.62683+cablesized/2),a/2-(12.68/2),0])
cylinder (h = 20,r =3, $fn = 6);
}
}

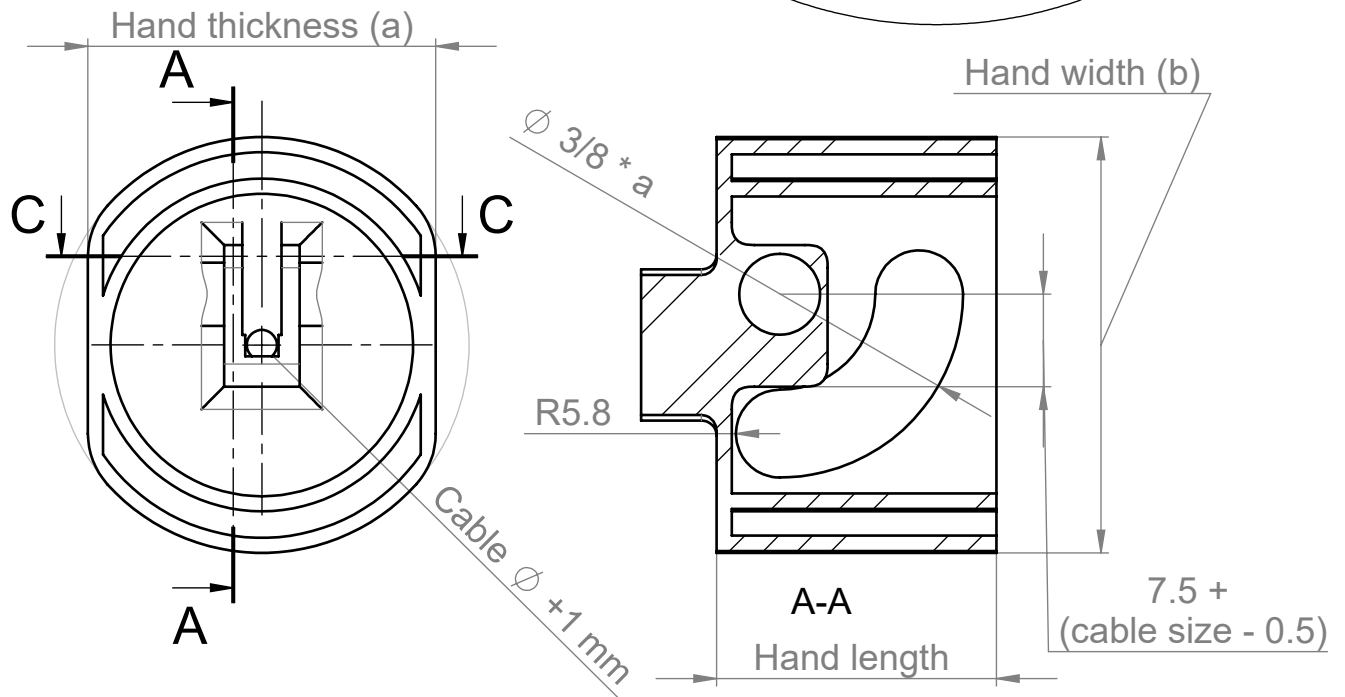
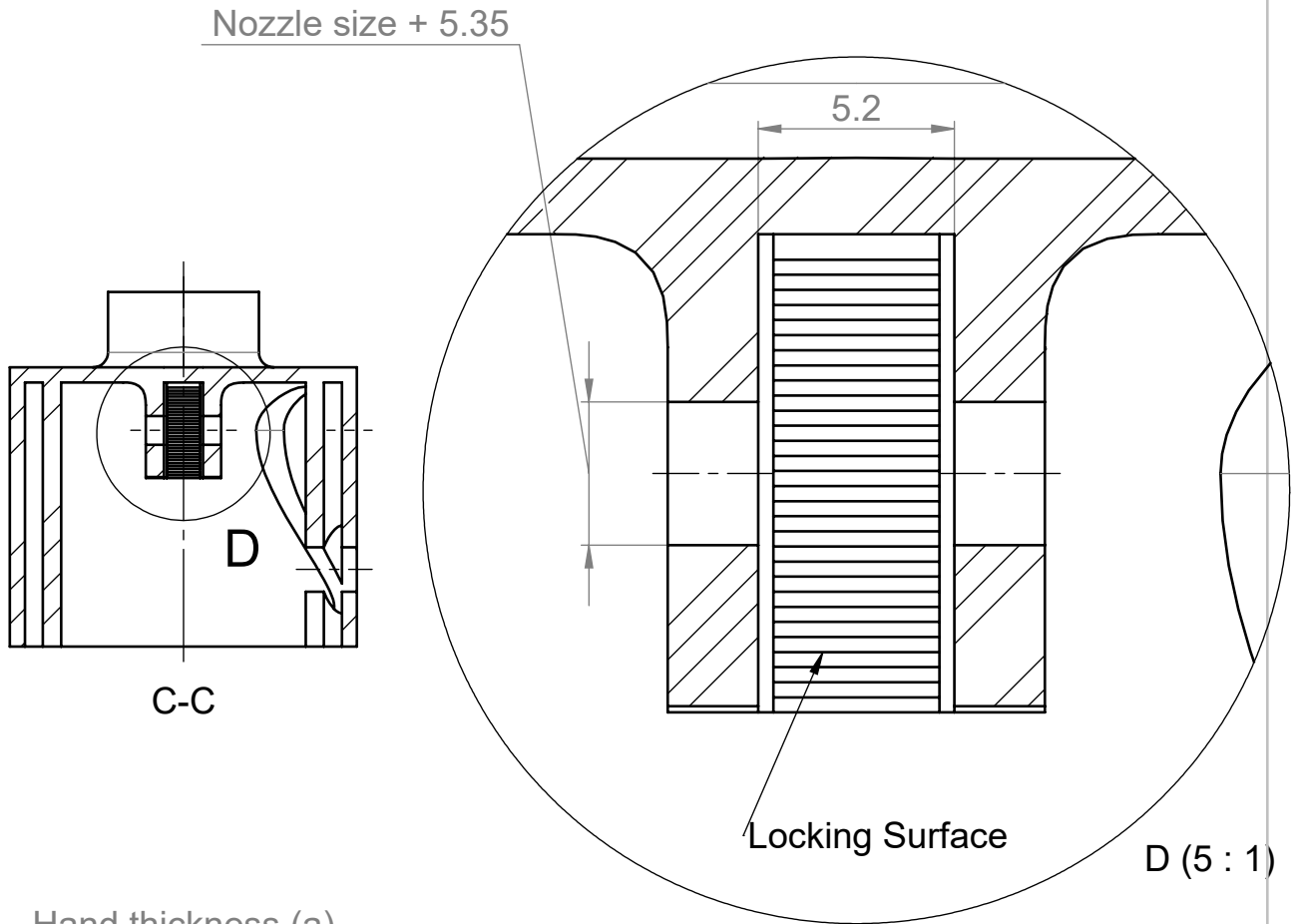
```

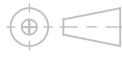
Mat.: PLA
3D Printed using FDM



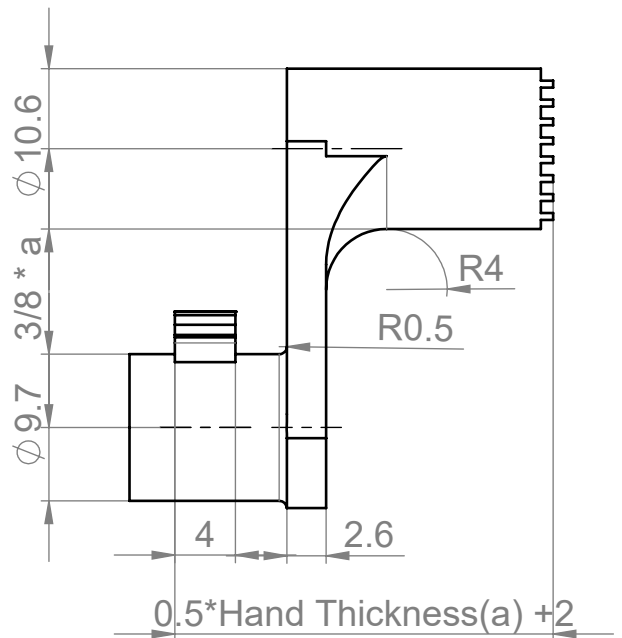
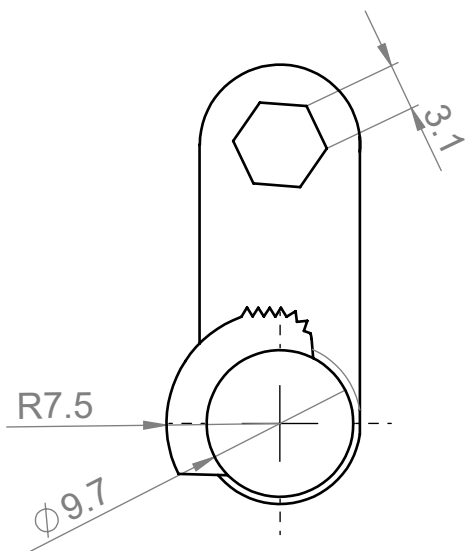
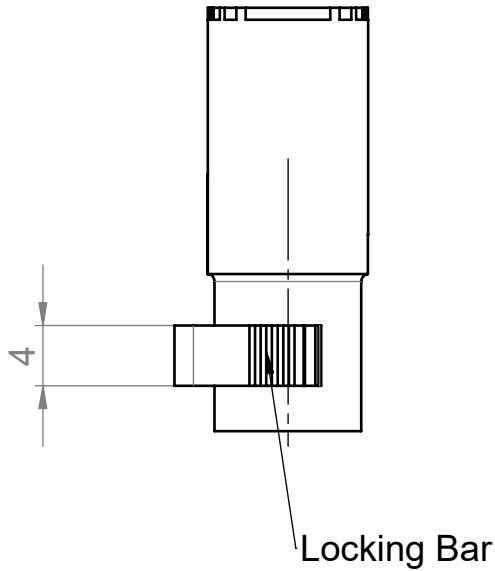
name		final v2		 units mm		
 TU Delft Industrial Design Engineering		scale	1:1	date	09-Nov-18	
		author	Andika Pradiya Hadiputra		weight	36 grams
				format	A4	
				units	mm	
				drawing no.	h	
				group	<<groep>>	

Mat.: PLA
3D printed using FDM process



name		shell		 units mm		
		scale	1:1	date	07-Nov-18	
Industrial Design Engineering		author	Andika Praditya Hadiputra		weight	33 grams
				format	A4	
					drawing no.	2
					group	SHELL

Mat.: PLA
3D Printed Using FDM process



name		locking bar		units mm	
format		A4		drawing no. 3	
scale 2:1		date 07-Nov-18		weight 3 grams	
author Andika Pradiya				group Locking Bar	
TU Delft Industrial Design Engineering					